ICIS'23
International Conference on Ion Sources
Victoria, BC, Canada

3D Self-Consistent Full-Wave PIC Models for Investigating Space-Resolved ECR Plasma Properties

B. Mishra, A. Galatà, A. Pidatella, G. Torrisi, C. Salvia, G.S. Mauro, E. Naselli, R. Ràcz, S. Biri and D. Mascali

Department of Physics and Astronomy "Ettore Majorana", University of Catania and INFN-LNS

PhD candidate under the supervision of David Mascali

ECR Ion Sources and PANDORA

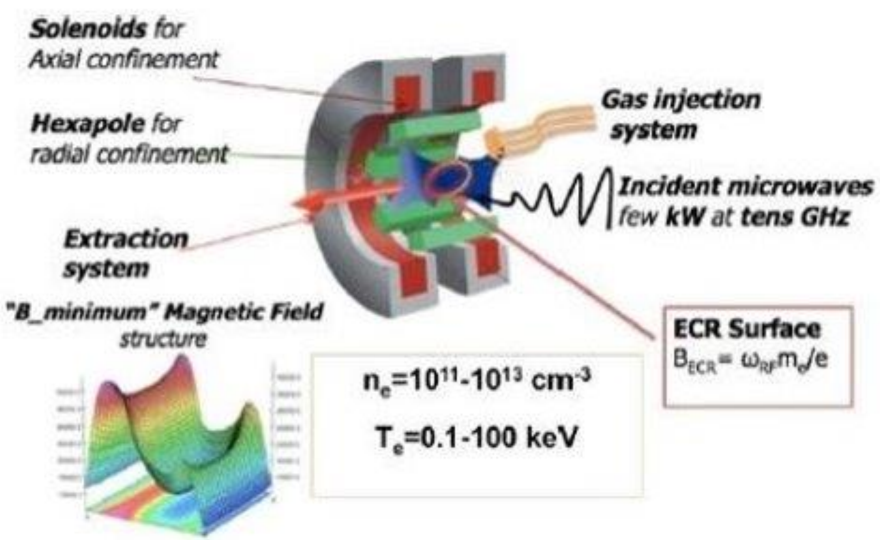

Schematic of ECRIS operation and global electron properties [1]

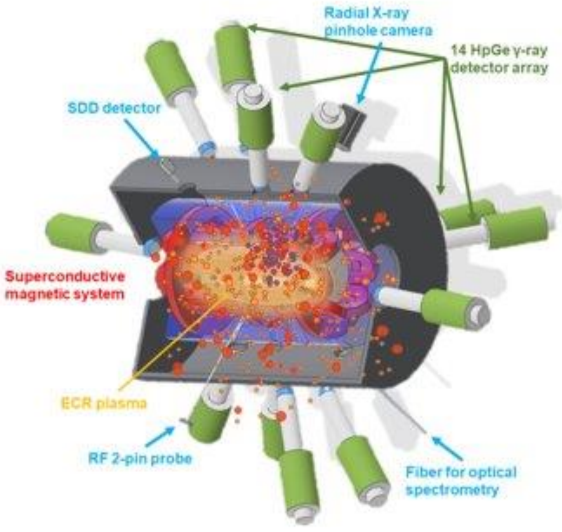

Schematic of PANDORA ECR plasma trap surrounded by HpGe detectors and diagnostics systems

ECR magnetic trap to study nuclear astrophysics in a plasma.

1. Modification of β-decay rates of radio-isotopes relevant to s-process nucleosynthesis
2. Opacity of heavy elements for modelling kilonovae light curves relevant to r-process nucleosynthesis

The shape and size of plasma chamber, pressure, RF power and frequency strongly influence

- Beam magnitude and current
- Plasma density and temperature distribution
- Susceptibility to instabilities

PANDORA – **P**lasmas for **A**strophysics, **N**uclear **D**ecay **O**bservations and **R**adiation for **A**rchaeometry

Ion CSD and LPD control the decay rates and opacity of radio-isotopes in the plasma

Talk by Eugenia Naselli on Sep 21!

[1] D. Mascali *et al.*, Eur. Phys. J. A 53, 145 (2017).

Measurement and Modelling Strategy

Simulations can be a powerful tool to predict 3D space-resolved properties of ECR plasma for fundamental and applied studies

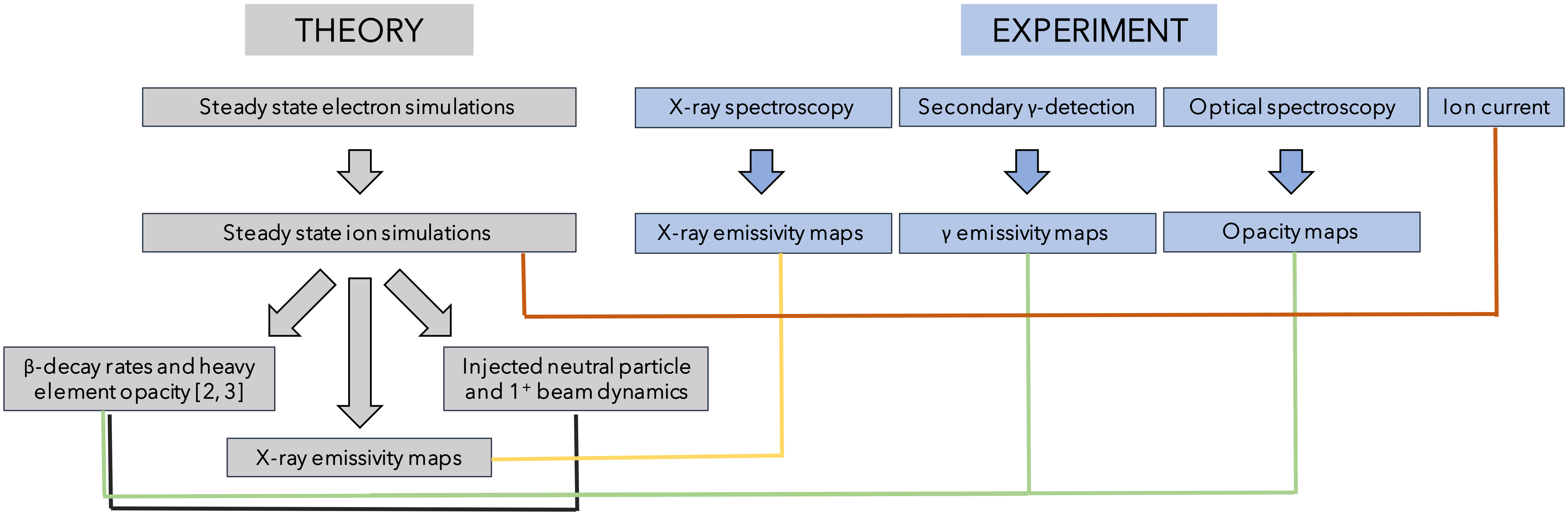

[2] K. Takahashi and K. Yokoi, Nucl. Phys. A 404, 1983 [3] A. Pidatella *et al*, Frontiers in Astronomy and Space Science 9:931744

Full-Wave Electron Kinetics

Schematic of COMSOL Multiphysics© + MATLAB© self-consistent numerical modelling for electrons

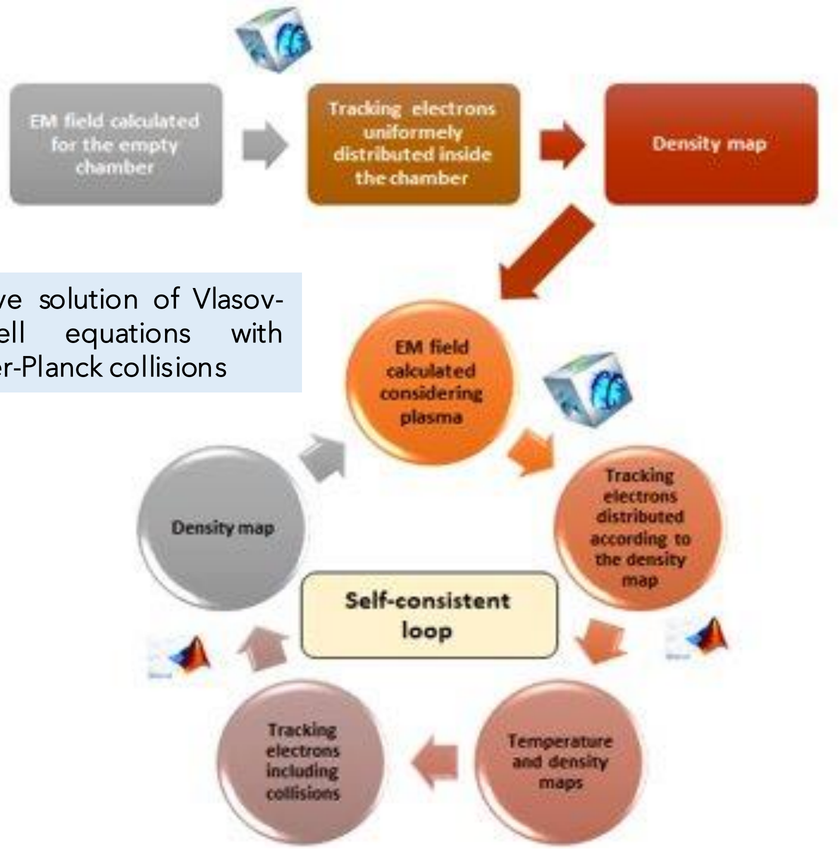

Iterative solution of Vlasov-Maxwell equations with Fokker-Planck collisions

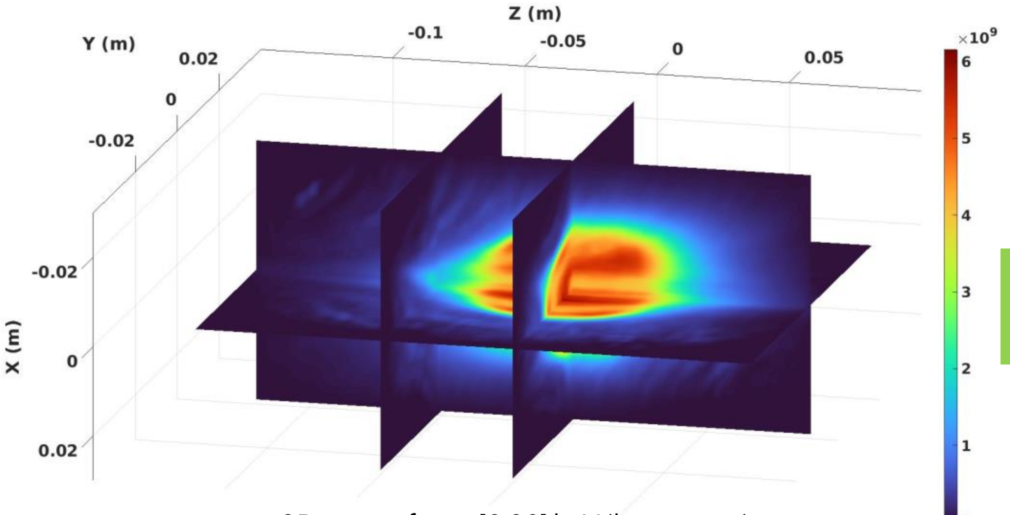

3D map of n_e in [0,30] keV (low power)

OPERATING CONDITIONS: 12.84 GHz, 30 W, Argon

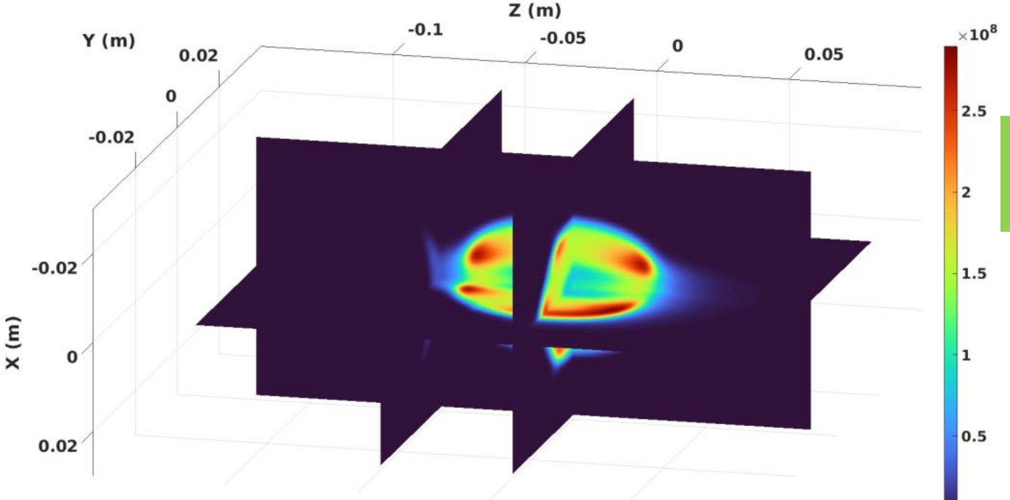

3D map of n_e in [1,100] keV (high power)

OPERATING CONDITIONS: 14.25 GHz, 200 W, Argon

See poster by Alessio Galatà!

[4] A. Galatà *et al*, Frontiers in Physics 10:947194, 2022

Full-Wave Electron Kinetics: Hot Electron Tensor

Wave-plasma coupling self-consistently modelled using "cold electron" approximation

- Electron speed << phase velocity of waves

Warm electron contribution to dielectric tensor substantial in ECR plasma

- Efforts underway to switch from cold electron to hot electron dielectric tensor

$$\bar{\bar{\varepsilon}} = \begin{pmatrix} \varepsilon_{xx} & \varepsilon_{xy} & \varepsilon_{xz} \\ \varepsilon_{yx} & \varepsilon_{yy} & \varepsilon_{yz} \\ \varepsilon_{zx} & \varepsilon_{zy} & \varepsilon_{zz} \end{pmatrix}$$

GENERAL FORM

Plasma dispersion function

$$\varepsilon_{ij} = \delta_{ij} - \sum_{\alpha} \Pi_{ij}^{\alpha} \sum_{n=-\infty} \Gamma_{ij}^{n}(\lambda_{\alpha}) Z_{ij}(x_{n\alpha})$$

Modified Bessel function of the first kind

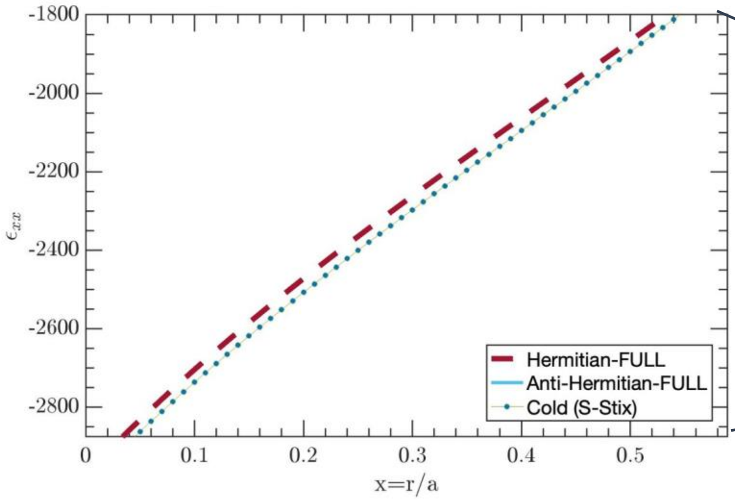

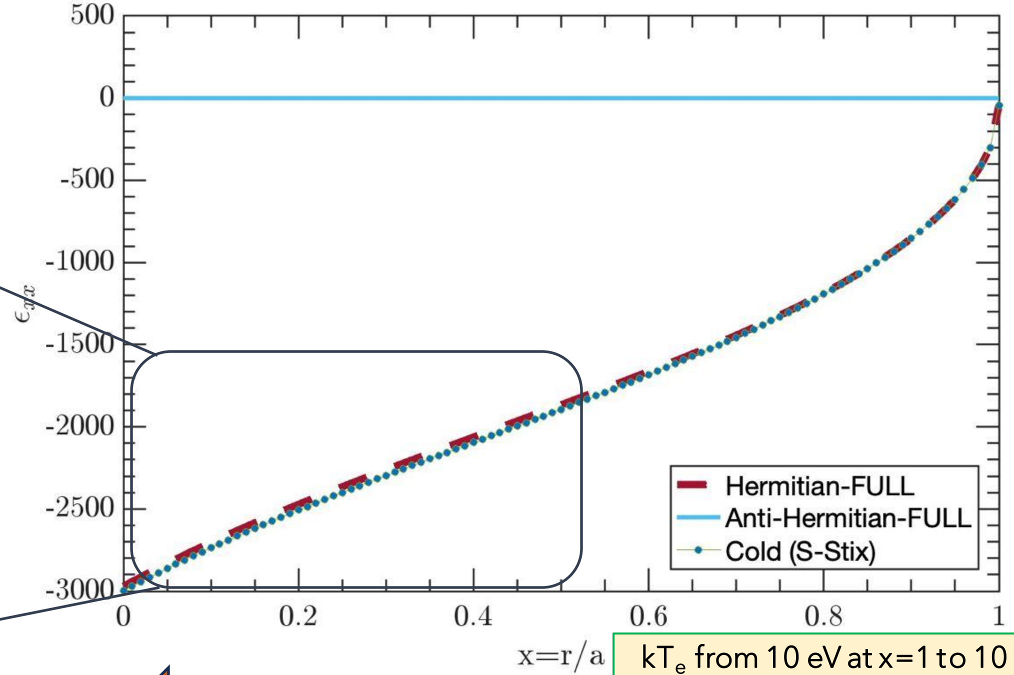

kT_e from 10 eV at x=1 to 10 keV at x=0

Self-Consistent Ion Kinetics

Vlasov-Maxwell equations + Fokker-Planck Collisions + Balance Equation

BUFFER IONS BALANCE EQUATION: $$\boxed{\frac{\mathrm{d}n_i}{\mathrm{d}t} = n_{i-1}n_e\gamma_{i-1,i} - n_i n_e \gamma_{i,i+1} + n_{i+1}n_0 E_{i+1,i} - n_i n_0 E_{i,i-1} - \frac{n_i}{\tau_i}}$$

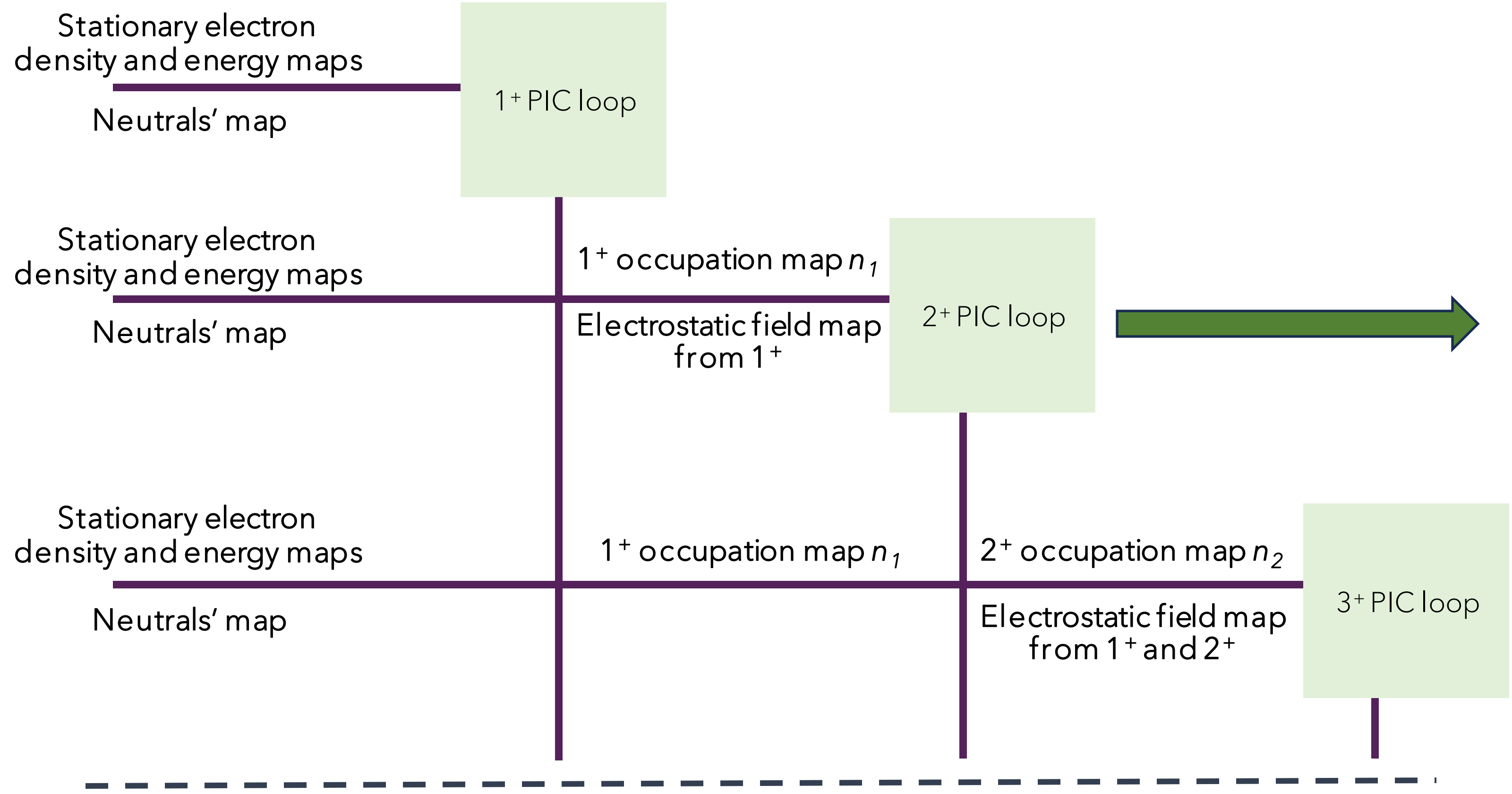

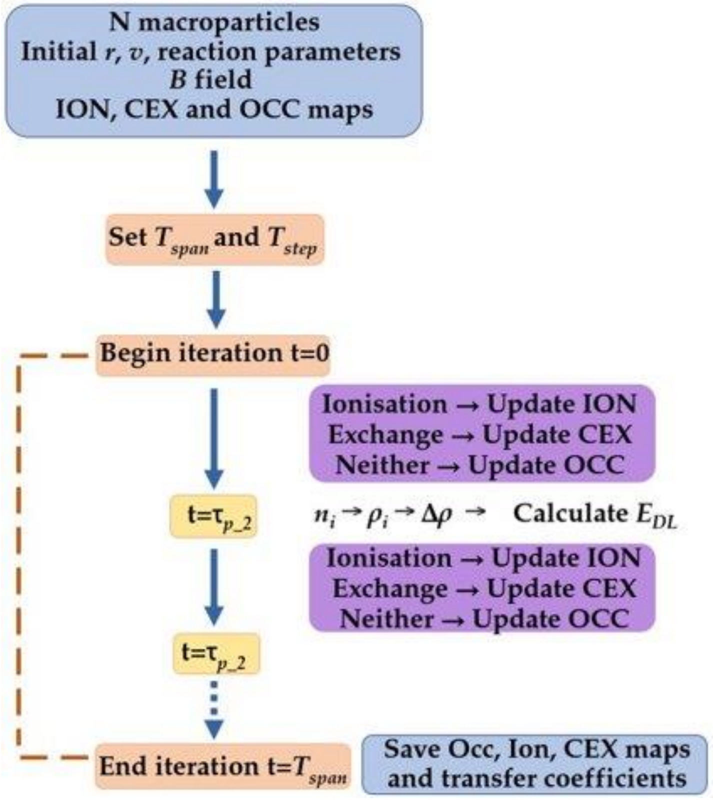

Till convergence...

Self-Consistent Ion Kinetics: Modules

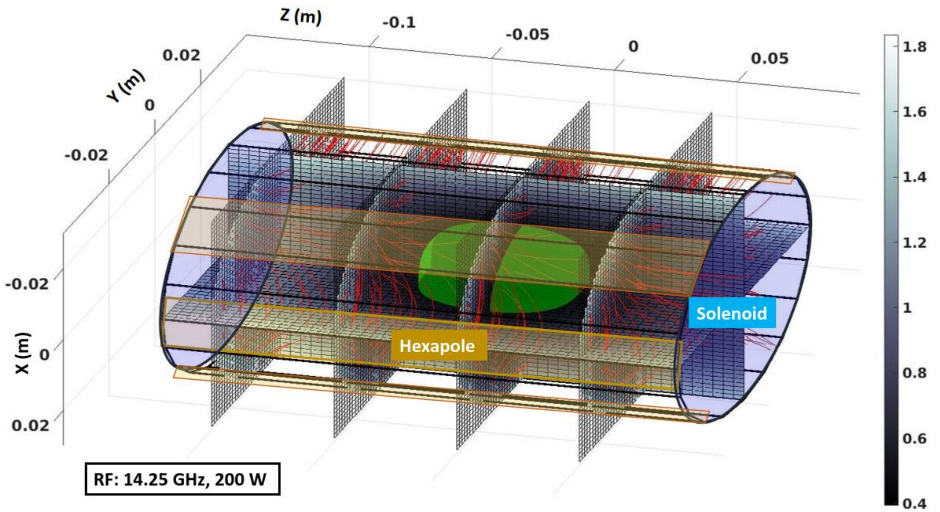

3D view of min-B profile with streamlines of field flow (top) [6]

BORIS METHOD

Set of equations for transporting particles under Lorentz force

LANGEVIN EQUATION

Formalism for including diffusion and friction forces for velocity evolution

MONTE CARLO SAMPLING

Formalism for sampling from multiple competing processes

$$\nu_{CEX} = n_0 \sigma_{CEX} v_i$$

Effective reaction frequency

$$P_{ion} = \frac{\nu_{ion}}{\nu_{tot}}(1 - e^{-\nu_{tot}\Delta T})$$

$$\nu_{ion} = n_e \sigma_{ion} v_e \qquad \nu_{tot} = \nu_{ion} + \nu_{CEX}$$

$$P_{CEX} = \frac{\nu_{CEX}}{\nu_{tot}}(1 - e^{-\nu_{tot}\Delta T})$$

CSD AND DENSITY SCALING

ION NUMBER DENSITY ⟷ ELECTRON NUMBER DENSITY

$$\oint_V n_e \mathrm{d}V = K_3 \Big[(1 - k_{1\to2} + 2k_{1\to2}k_{2\to1} + k_{1\to2}k_{2\to3}k_{3\to2}) \oint_V n_1 \mathrm{d}V +$$
$$2k_{1\to2}(1 - k_{2\to3} - k_{2\to1} + k_{2\to3}k_{3\to2}) \oint_V n_2 \mathrm{d}V +$$
$$3k_{1\to2}k_{2\to3}(1 - k_{3\to4} - k_{3\to2}) \oint_V n_3 \mathrm{d}V +$$
$$4k_{1\to2}k_{2\to3}k_{3\to4} \oint_V n_{3\to4} \mathrm{d}V \Big]$$

Transfer coefficients

Conservation of total charge

[5] B. Mishra *et al*, Frontiers in Physics 10:932448, 2022 [6] B. Mishra, EPJ Web of Conferences 275, 02001, 2023
[7] A. Galatà *et al,* PSST 25, 045007, 2016 [8] A. Galatà *et al,* Rev. Sci. Instrum. 91, 013506, 2019

Model Predictions: CSD and Ion Current

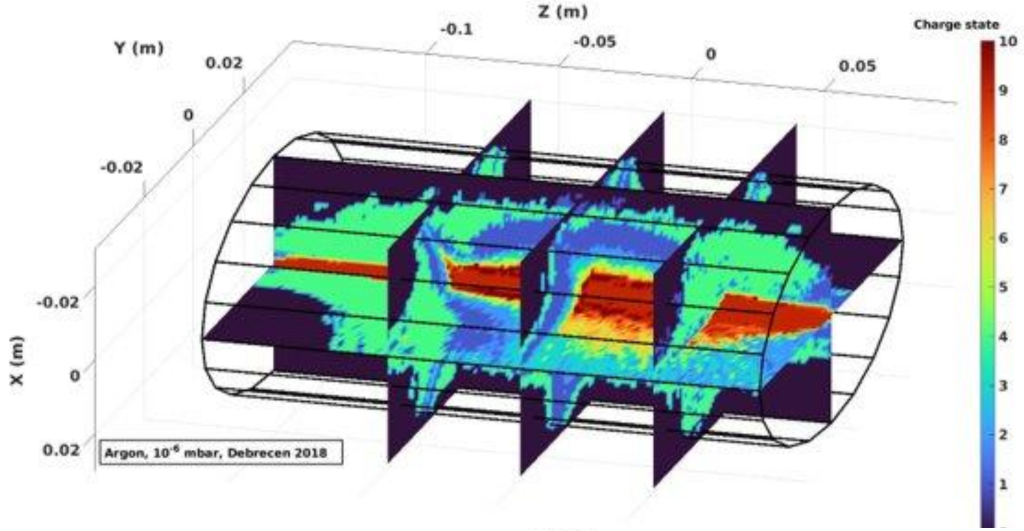

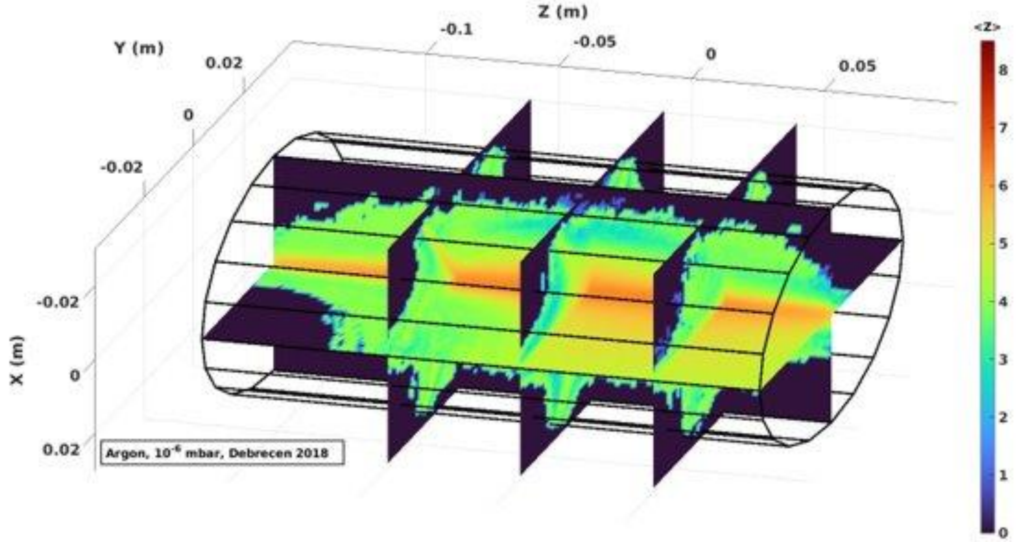

Regions of peak occupancy of each charge state (top) and 3D distribution of mean charge state of plasma [6] (bottom)

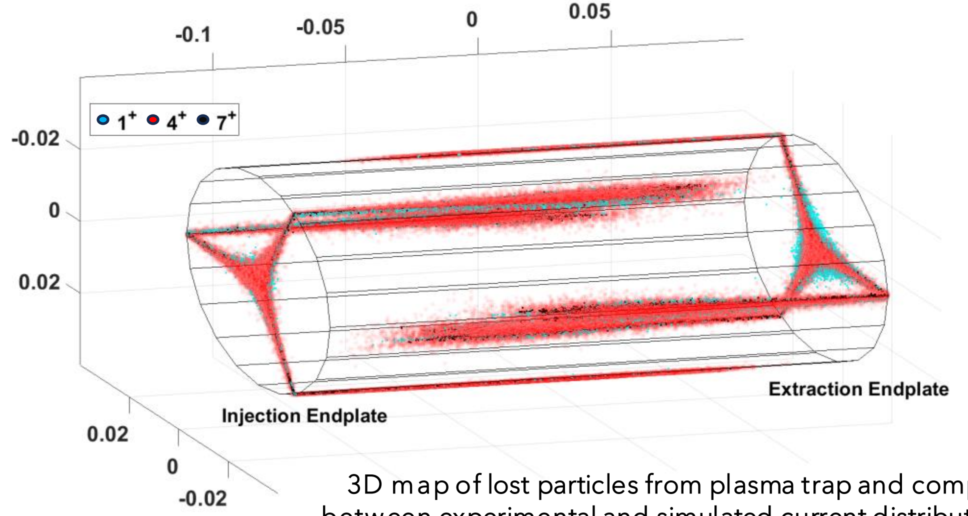

3D map of lost particles from plasma trap and comparison between experimental and simulated current distribution [5, 6]

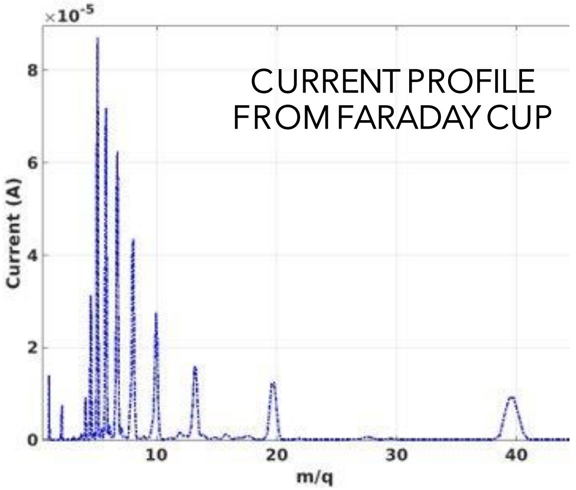

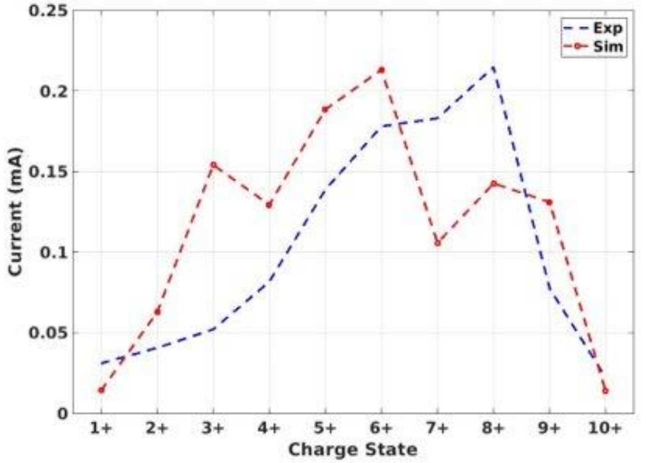

[5] B. Mishra *et al*, Frontiers in Physics 10:932448, 2022 [6] B. Mishra, EPJ Web of Conferences 275, 02001, 2023
[9] S. Biri *et al,* Rev. Sci. Instrum. 83, 02A431, 2012

Model Predictions: X-Ray Emissivity Maps

$$C = T\rho_e\rho_i\omega_{K\alpha}\varepsilon_g\varepsilon_q \int_I^{\infty} \sigma_{K,ion}(E)v_E f(E)\mathrm{d}E$$

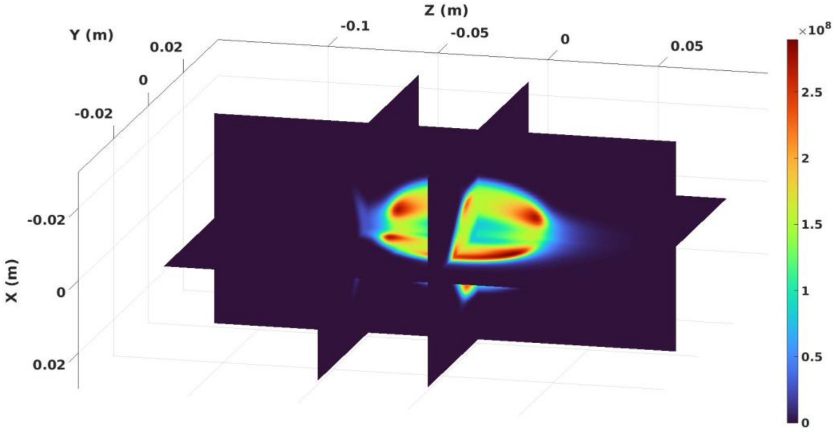

Electron density maps

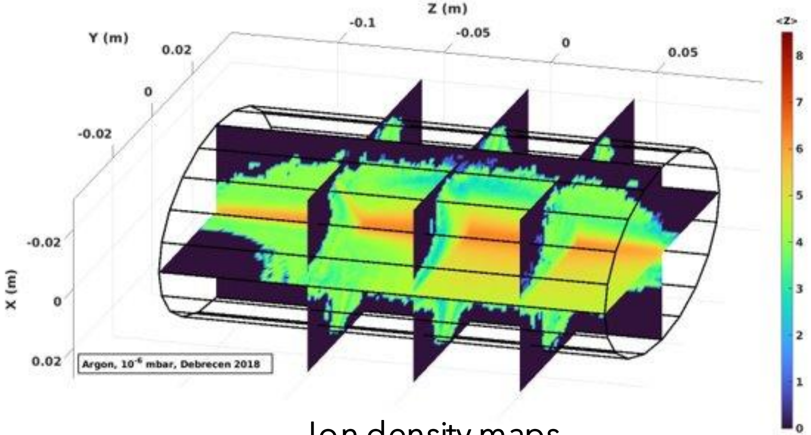

Ion density maps

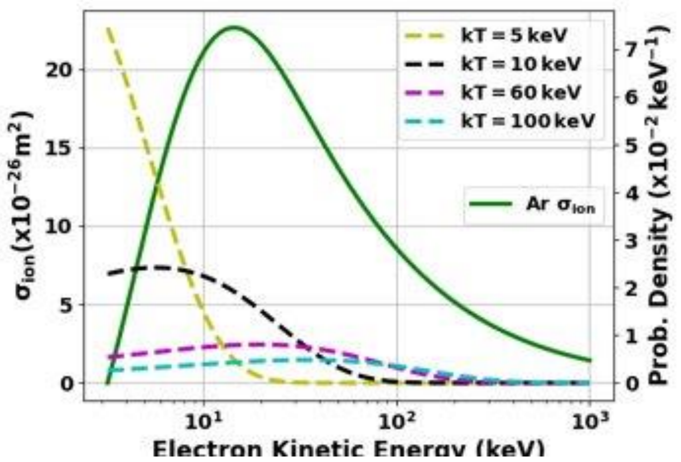

Cross sections

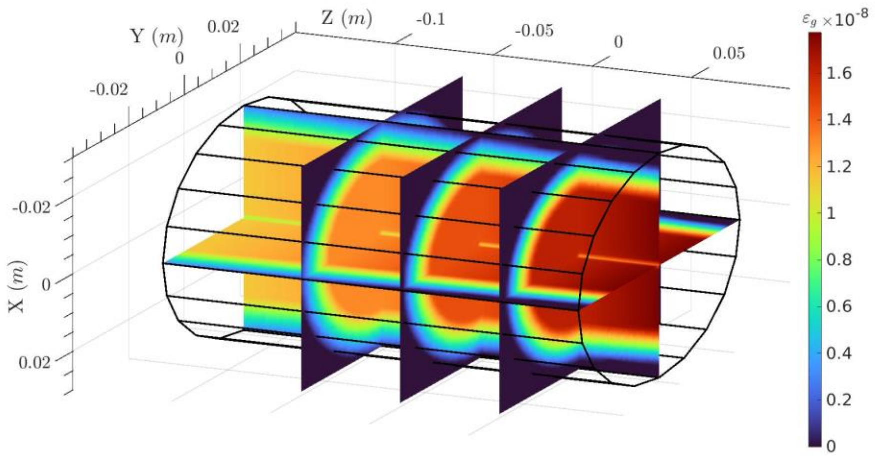

Geometrical efficiency

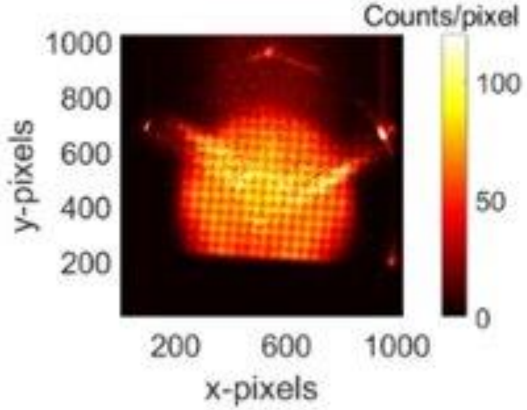

Comparison between experimental [12] and simulated fluorescence maps

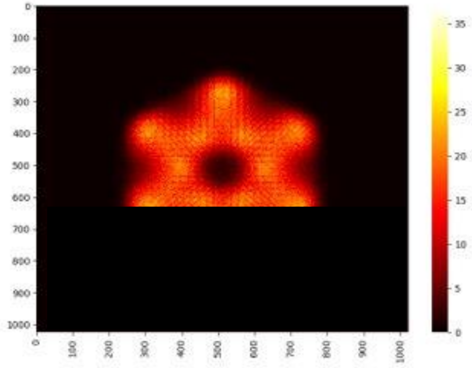

[10] B. Mishra *et al*, Phys. Plasmas 2021
[11] B. Mishra, Condensed Matter 2021
[12] S. Biri *et al*, JINST 16, P03003 2021

Model Predictions: β-Decay Rate Maps

$$({}^A_Z X_N)^{i,j} \rightarrow ({}^{A}_{Z+1}Y_{N-1})^{i+1,j'} + e^-_f + \bar{\nu}_e$$

$$({}^A_Z X_N)^{i,j} \rightarrow ({}^{A}_{Z+1}Y_{N-1})^{i,j'} + e^-_b + \bar{\nu}_e$$

$$({}^A_Z X_N)^{i,j} + e^-_f \rightarrow ({}^{A}_{Z-1}Y_{N+1})^{i,j'} + \nu_e$$

$$({}^A_Z X_N)^{i,j} + e^-_b \rightarrow ({}^{A}_{Z-1}Y_{N+1})^{i-1,j'} + \nu_e$$

DECAY CHANNELS

NEUTRAL ATOM Q-VALUE

$$Q_0 = \begin{cases} m_0({}^A_Z X_N)c^2 - m_0({}^{A}_{Z+1/Z-1}Y_{N-1/N+1})c^2 \\ m_0({}^A_Z X_N)c^2 - m_0({}^{A}_{Z+1/Z-1}Y_{N-1/N+1})c^2 + K_{e^-_f} \end{cases}$$

IONISED ATOM Q-VALUE

$$Q = Q_0 + (E^*_{X,K} - E^*_{Y,K'}) + (\epsilon^{i,j} - \epsilon^{i',j'}) + (\Delta_X - \Delta_Y)$$

DECAY FT-VALUE

$$f_{if(m)}t_{1/2} = \frac{(\ln 2)2\pi^3\hbar^7}{g^2 m_e^5 c^4 |M_{if}^{L(m)}|^2}$$

LEPTON PHASE VOLUME

$$f^*_{IF(m)} = \sum_{ij} p_{ij} \sum_{x(ij)} \sigma_x \frac{\pi}{2}[g_x\, or\, f_x]^2 (Q(ij)/m_e c^2)^2 S_{(m)x(ij)}$$

IN-PLASMA DECAY RATE

$$\boxed{\lambda_{tot} = \sum \frac{\ln 2}{f_{IF(m)}t_{1/2}} f^*_{IF(m)}}$$

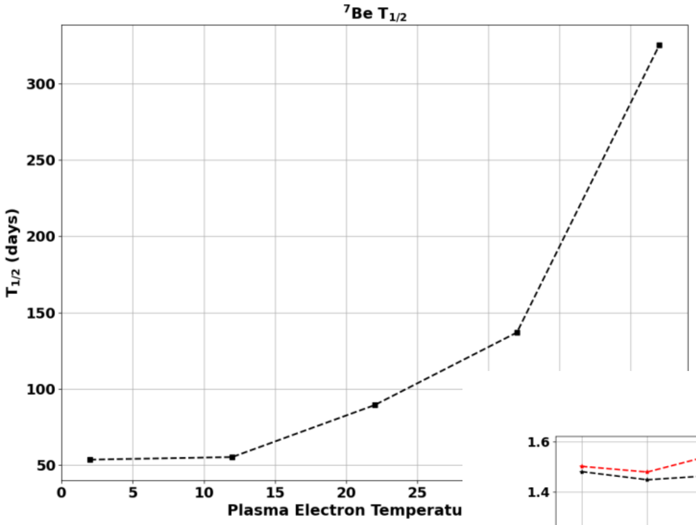

^{7}Be half-life variation as a function of plasma temperature

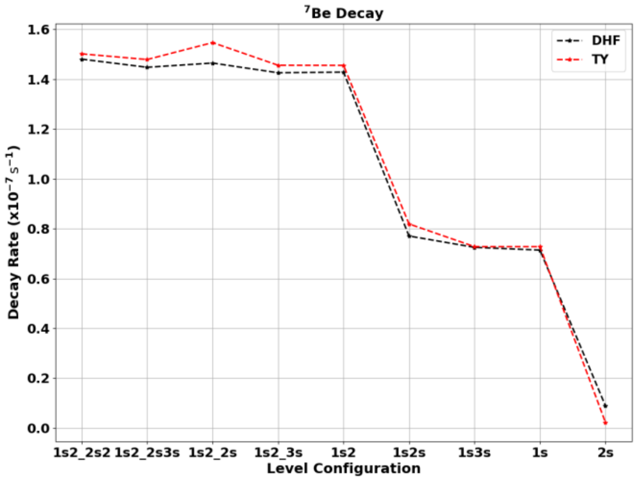

^{7}Be half-life variation as a function of electronic configuration in ions

Model Predictions: β-Decay Rate Maps

Vlasov-Maxwell equations + Fokker-Planck Collisions + Balance Equation

ISOTOPE IONS BALANCE EQUATION:

$$\frac{dn_i^R}{dt} = \left[n_{i-1}^R n_e \gamma_{i-1,i} - n_i^R n_e \gamma_{i,i+1}\right] + \left[n_{i+1}^R \sum_{j=0}^{N-1} n_j E_{i+1,i} + n_{i-1}^R \sum_{j=1}^{N} n_j E_{i-1,i}\right] - \left[n_i^R \sum_{j=0}^{N-1} n_j E_{i,i-1} + n_i^R \sum_{j=1}^{N} n_j E_{i,i+1}\right] - \frac{n_i^R}{\tau_i^R}$$

$$\frac{dn_{ii'}^R}{dt} = \left[\sum_{ij'<ii'} n_{ij'}^R n_e C_{ij'ii'} - n_{ii'}^R \sum_{ij'>ii'} n_e C_{ii'ij'}\right] + \left[\sum_{ij'>ii'} n_{ij'}^R A_{ij'ii'} - n_{ii'}^R \sum_{ij'<ii'} A_{ii'ij'}\right]$$

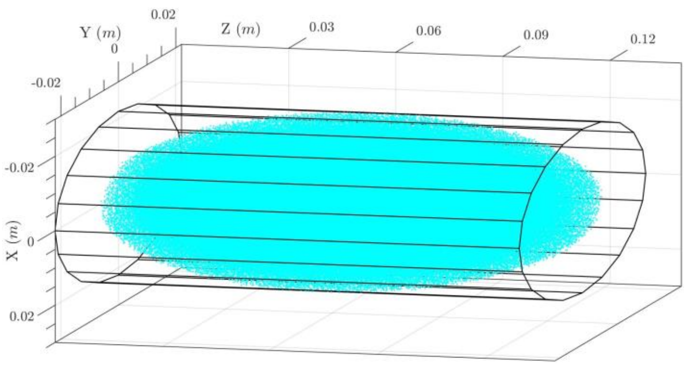

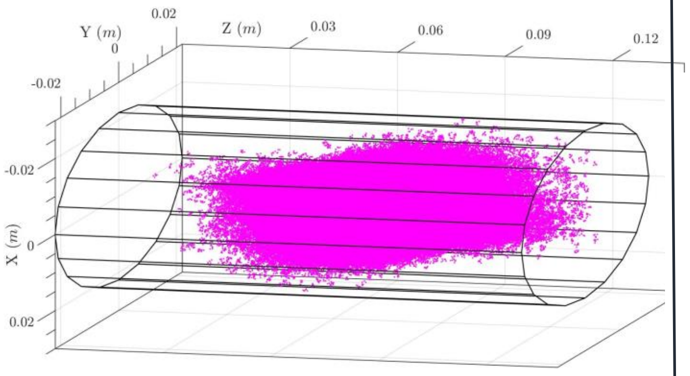

Distribution of macroparticles corresponding to 0^+ and 2^+ charge states of ^7Be

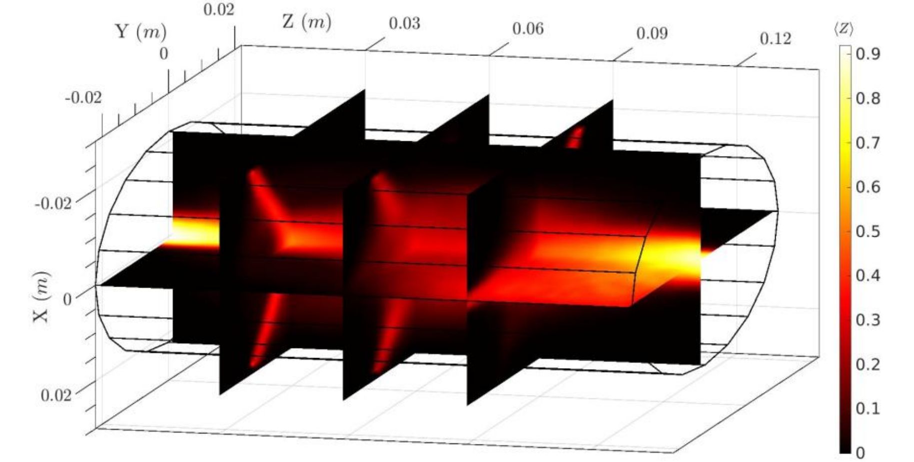

Mean charge map of 7Be in the plasma trap (top) and corresponding $T_{1/2}$ map (bottom)

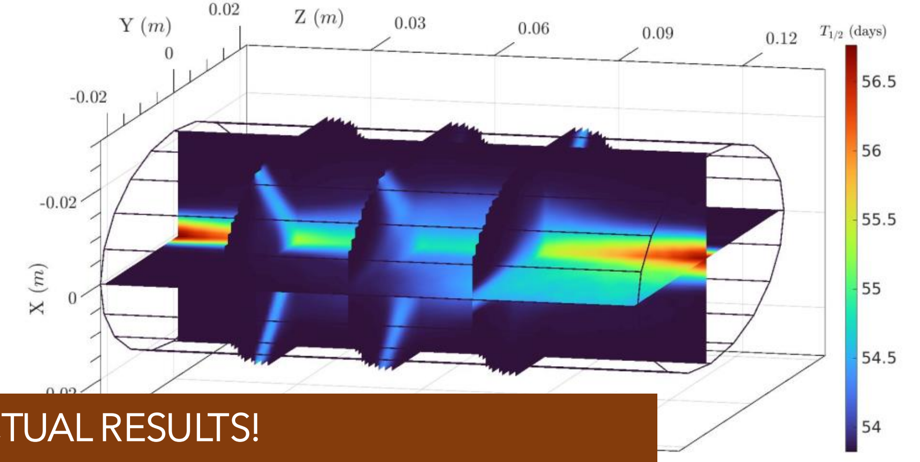

PROOF OF CONCEPT SIMULATION, NOT ACTUAL RESULTS!

PANDORA trap is optimised to produce high charge states and much greater variation in $T_{1/2}$

Model Predictions: Neutral Particle Dynamics

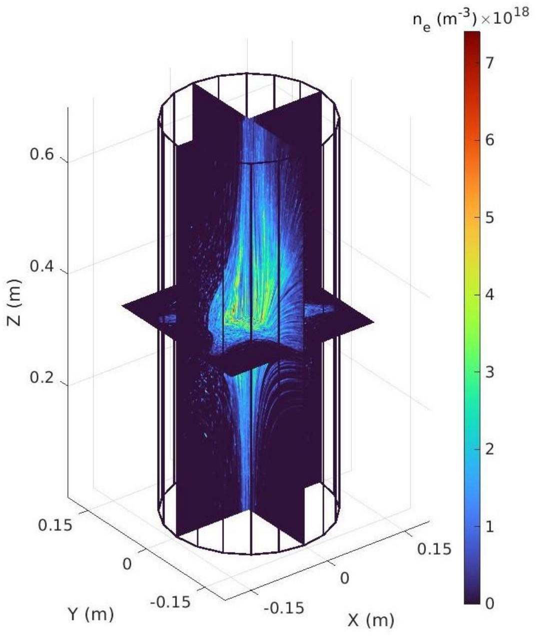

Electron maps from full-wave PIC codes

➕ ION KINETICS PIC CODE

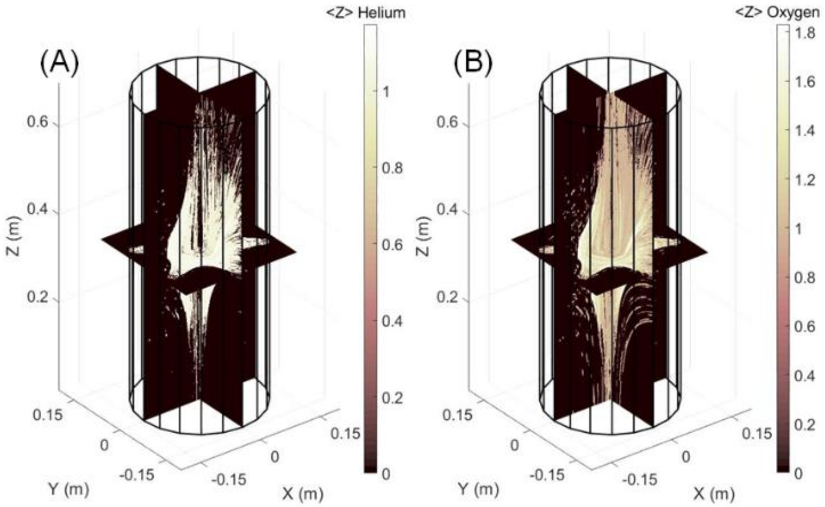

Ion maps for different species

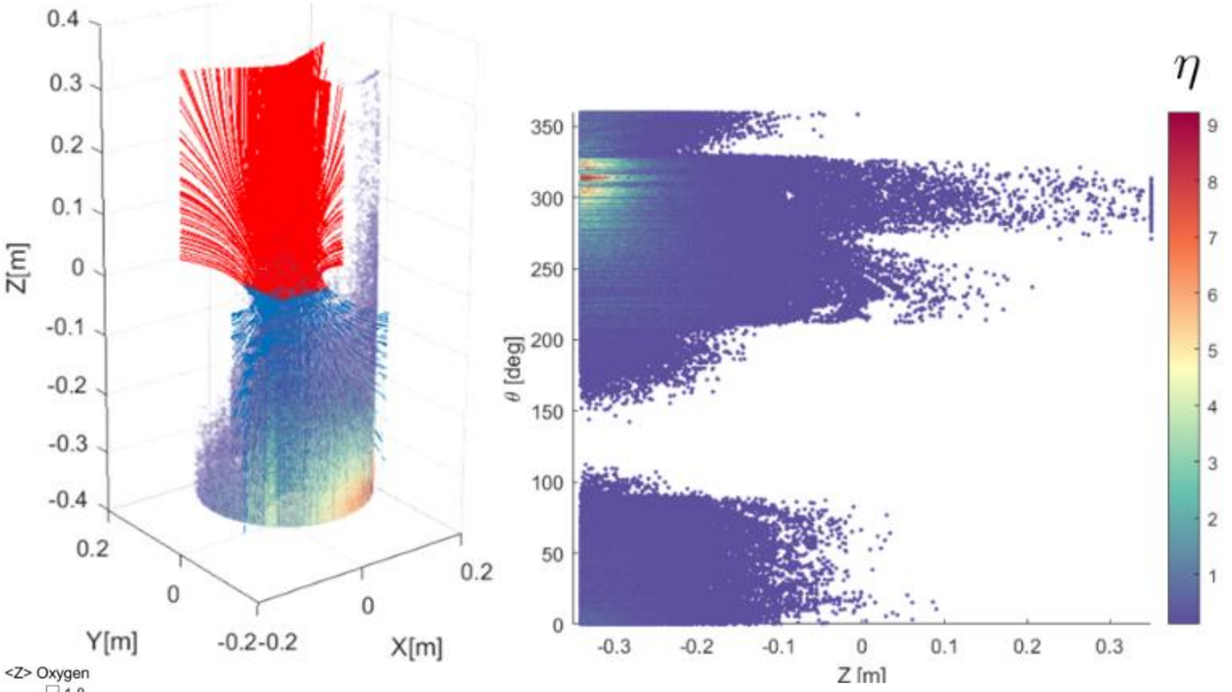

Deposition of injected neutral particles on the plasma wall, indicating regions of capture from different processes [13]

See poster by Angelo Pidatella!

[13] A. Pidatella *et al*, Metal evaporation dynamics in Electron Cyclotron Resonance Ion Sources: plasma role in the atom diffusion, conversion to ion, and transport, submitted to PPCF

Conclusions and Perspectives

- ECR ion sources are useful for generating ion currents with tunable magnitude and charge states, but their internal plasma structure is complicated
- Full-wave PIC codes which evolve density with EM field distribution can furnish space-resolved maps of electron density and energy
- The algorithm is now being updated to shift from cold to hot electron tensor
- PIC-MC codes which solve ion balance equation self-consistently with electron charge distribution can furnish space-resolved maps of CSD and excitation levels
- Together these maps are powerful predictive tools to study numerous ECR plasma phenomena like X-ray emission, heavy element opacity and neutral particle dynamics
- These simulations can improve fundamental understanding of the operation of ECR ion sources (instabilities, current generation) as well as for applications involving them (PANDORA facility)

Sandor Biri
Richard Rácz

David Mascali
Domenico Santonocito
Angelo Pidatella
Eugenia Naselli
Giorgio Finocchiaro
Giuseppe Torrisi
Giorgio Mauro
Claudia Salvia

Alessio Galatà

Alessandro Cardinali

THANK YOU FOR YOUR ATTENTION!!!

Additional Slides

High energy bremsstrahlung and contribution from extraction plate

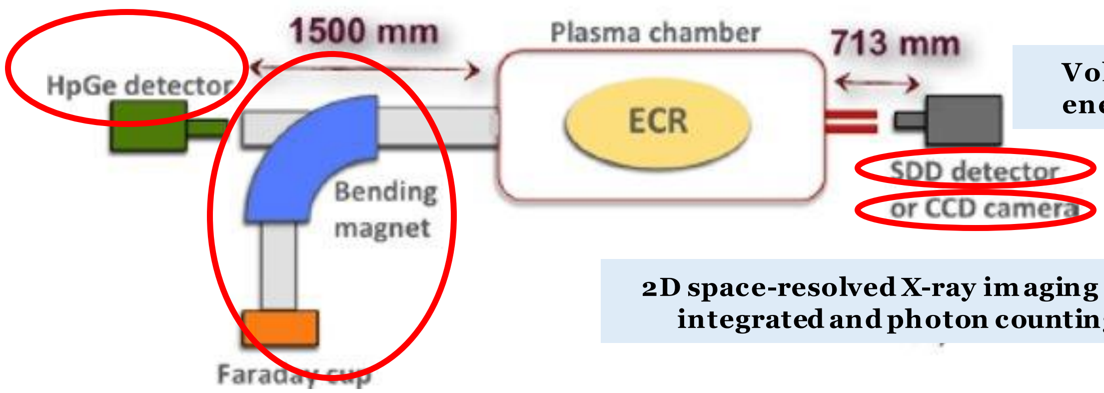

Volumetric fluorescence and low energy bremsstrahlung emission

2D space-resolved X-ray imaging (spectrally integrated and photon counting mode)

Measuring ion currents (total and individual charge states)

Schematic of Debrecen experimental setup showing various detectors used and distances [4]

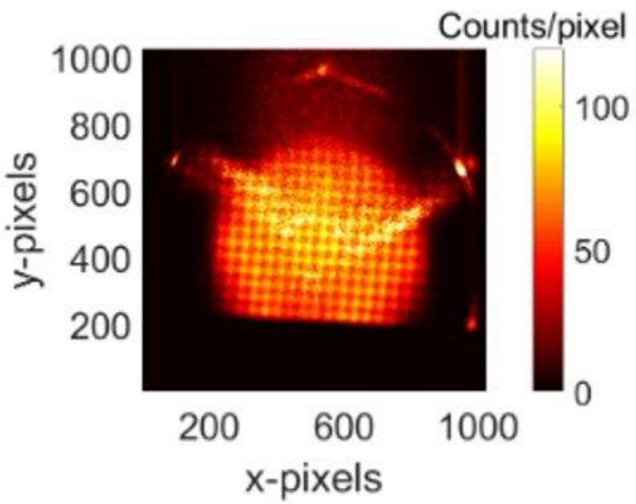

Ar Kα fluorescence image for Debrecen 2018

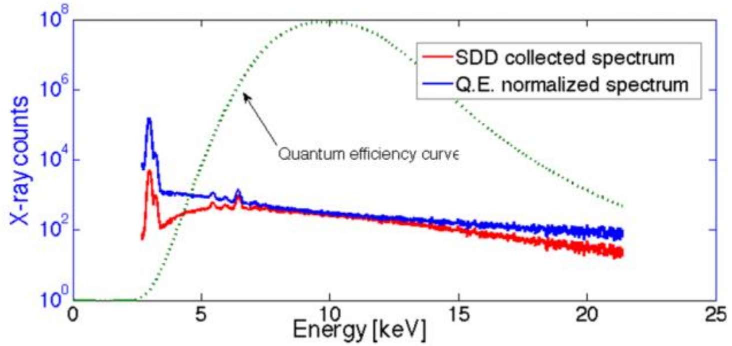

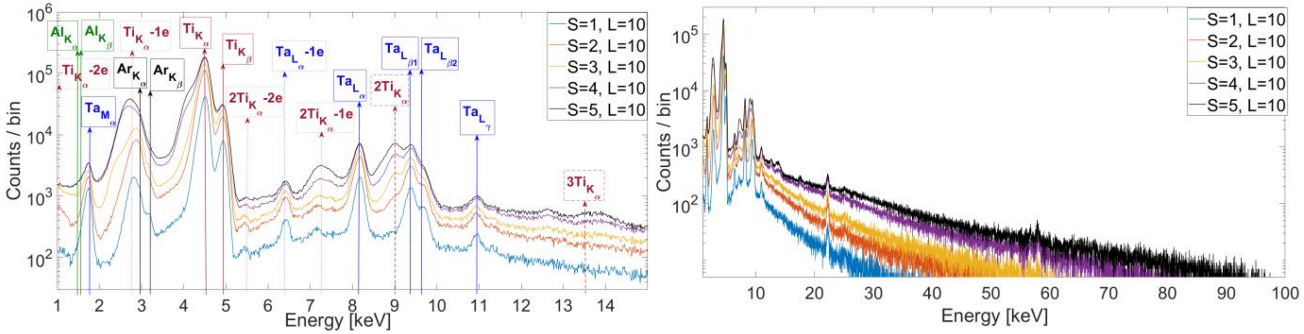

D. Mascali et al, Rev. Sci. Instrum. 87, 02A510 (2016).
E. Naselli et al, Condens. Matter 1, 0 (2021).

SDD volumetric spectrum from Debrecen 2014 (left) and spectrum from CCD pixel from Debrecen 2018 (right)

Additional Slides

$$T = 300\boxed{\rho_e \rho_i}\omega_{K\alpha}\boxed{\varepsilon_g \varepsilon_q}\int_{3.205}^{\infty}\boxed{\sigma_{K,ion}(E)}v(E)\boxed{f(E)}\mathrm{d}E$$

Electron and ion density – free parameter

Evaluating 3D space-resolved electron energy distribution function (EEDF) and analysing behaviour of K-shell ionisation cross-section

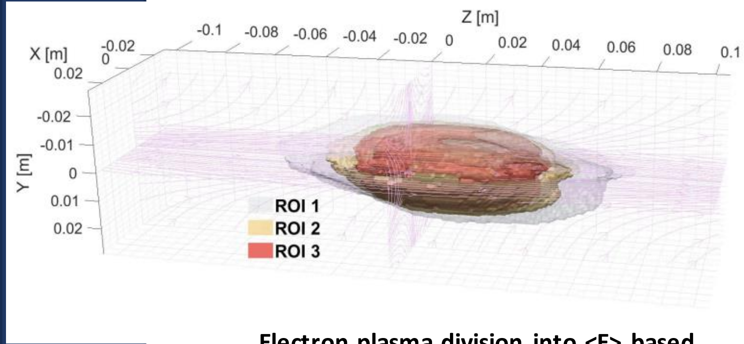

Electron plasma division into <E> based ROIs

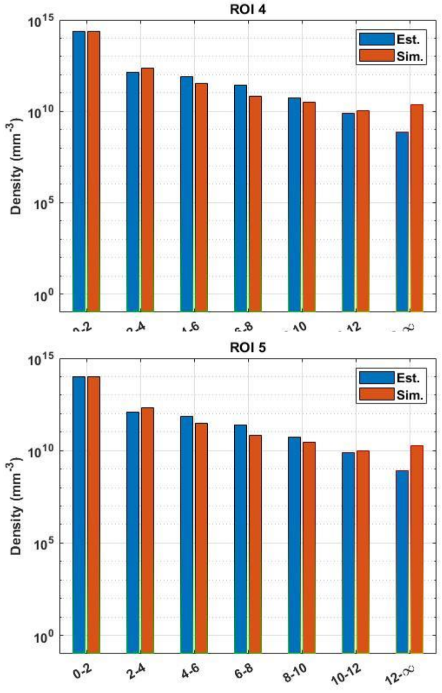

Maxwell + Druyvesteyn EEDF fit in various ROIs

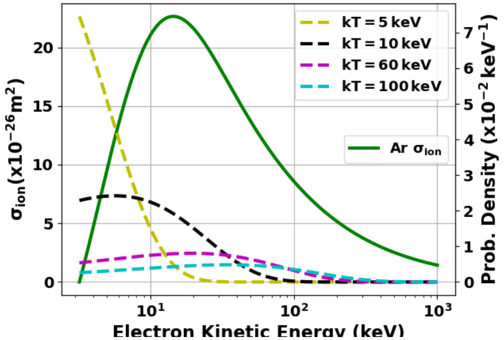

K-shell ionisation cross section for Ar (Lotz Formula) [6]

B. Mishra *et al*, Phys. Plasmas, (2021)
B. Mishra *et al*, Condens. Matter, (2021)
R. Racz *et al*, Plasma Sources Sci. Technol. 26, 075011 (2017)

Evaluating 3D space-resolved geometrical efficiency and quantum efficiency of simulation domain

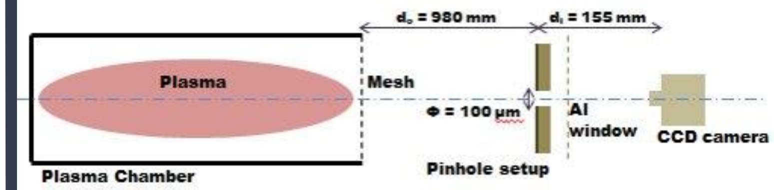

Schematic of CCD-pinhole setup

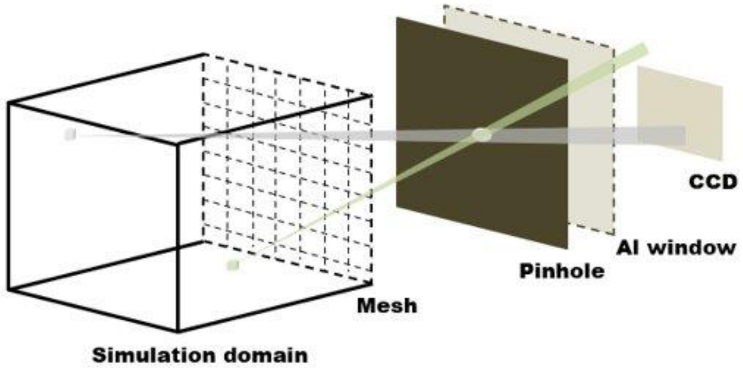

Ray-tracing MC code for geometrical efficiency

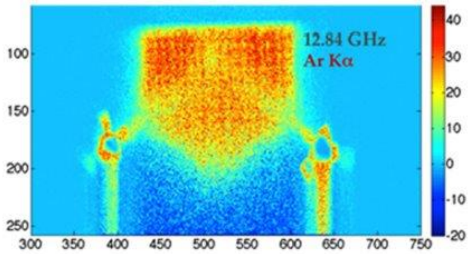

Experimental Kα fluorescence CCD image vs simulated emission map

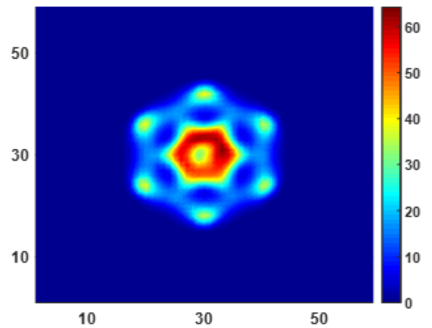

Additional Slides

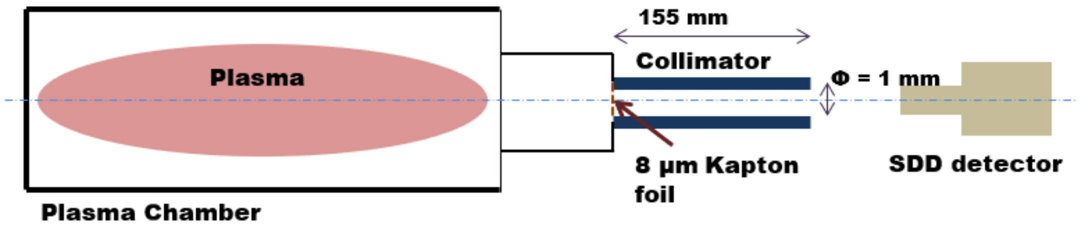

Schematic of experimental setup showing usefulness of collimator in filtering out emission from the walls/extraction plate

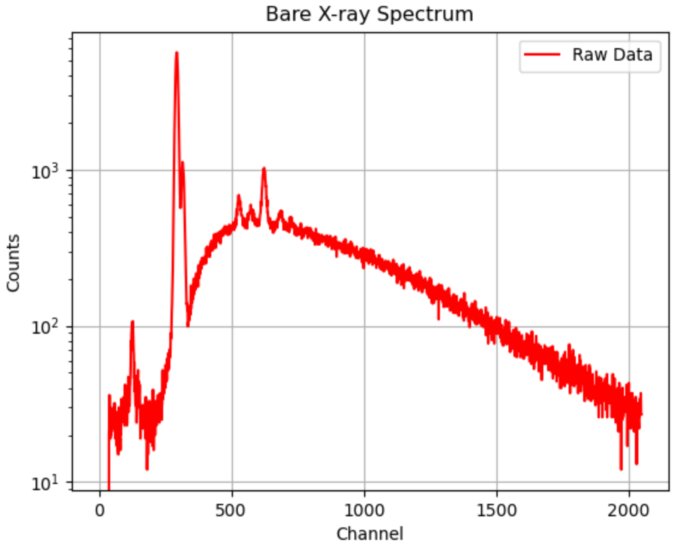

- **Calibration with Fe lines**
- **QE renormalisation**
- **Dead time correction**
- **Conversion to emissivity density**

$$J(h\nu) = h\nu \frac{N^p(h\nu)}{t} \frac{4\pi}{\Delta E V_P \Omega_g}$$

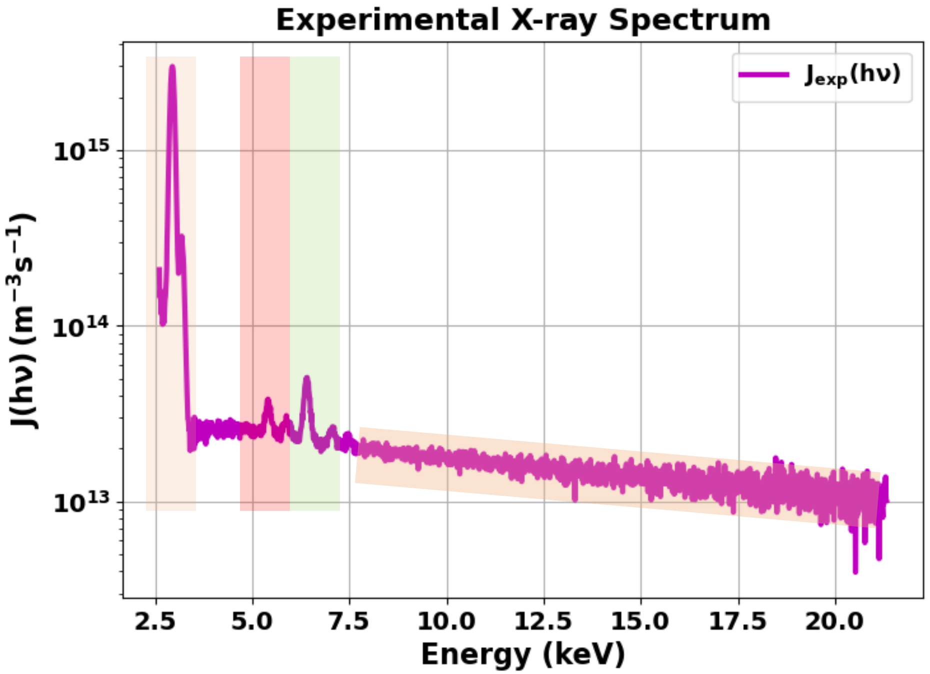

Contribution from bremsstrahlung, Ar fluorescence (confined electrons) and Cr/Fe fluorescence (escaping electrons)

B. Mishra *et al*, Condens. Matter, (2021)

Additional Slides

Bremsstrahlung Emissivity Density

$$J_{theo,brem}(h\nu) = \rho_e \rho_i \int_{h\nu}^{\infty} \frac{\mathrm{d}\sigma_K(h\nu)}{\mathrm{d}h\nu} v_e(E) f(E) \mathrm{d}E$$

⇩

Kramer's formula for differential cross section

$$\frac{\mathrm{d}\sigma_K(h\nu)}{\mathrm{d}h\nu} = \frac{16\pi}{3\sqrt{3}} \alpha^3 \left(\frac{\hbar}{m_e c}\right)^2 \left(\frac{c}{v_e}\right)^2 \frac{Z^2}{h\nu}$$

⇩

Single-component Maxwell EEDF

$$f_M(E; k_B T_e) = \frac{2}{\sqrt{\pi}} \frac{\sqrt{E}}{(\sqrt{k_B T_e})^3} e^{-E/k_B T_e}$$

⇩

$$J_{theo,brem}(h\nu) = \rho_e \rho_i (Z\hbar)^2 \left(\frac{4\alpha}{\sqrt{6 m_e}}\right)^3 \left(\frac{\pi}{k_B T_e}\right)^{1/2} e^{h\nu/k_B T_e}$$

B. Mishra *et al*, Phys. Plasmas, (2021)

Line Emissivity Density (Ar ions)

$$J_{theo,2.96} = \frac{h\nu_{2.96}}{\Delta E} \rho_e \rho_i \omega_{2.96} \int_{3.205}^{\infty} \sigma_{K,ion}(E) v_e(E) f(E) \mathrm{d}E$$

$$J_{theo,3.19} = \frac{h\nu_{3.19}}{\Delta E} \rho_e \rho_i \omega_{3.19} \int_{3.205}^{\infty} \sigma_{K,ion}(E) v_e(E) f(E) \mathrm{d}E$$

⇩

Lotz formula for K-shell ionisation cross-section

$$\sigma_{K,ion} = a_K q_K \frac{\ln \varepsilon / I}{\varepsilon I} \{1 - b_K \exp[-c_K(\varepsilon/I - 1)]\}$$

⇩

Pseudo-Voigt profile for line broadening

$$D_{PV}(x - x_0, f) = \eta L(x - x_0, \tau_L) + (1 - \eta) G(x - x_0, \sigma_G)$$

⇩

$$J_{theo,line,plasma}(h\nu) = [J_{theo,2.96} D_{PV}(h\nu - 2.96, f_{2.96}) + J_{theo,3.19} D_{PV}(h\nu - 3.19, f_{3.19})] \Delta E$$

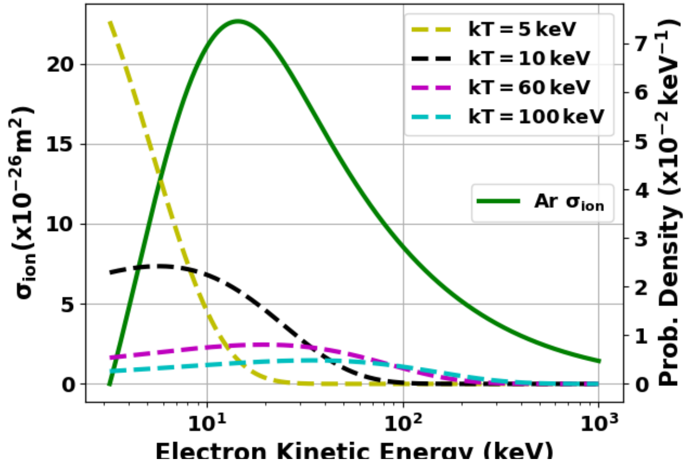

Lotz cross-section for Ar superposed on Maxwell EEDFs at different temperatures [6]

Electron Diagnostics – X-Ray Spectroscopy - Volumetric

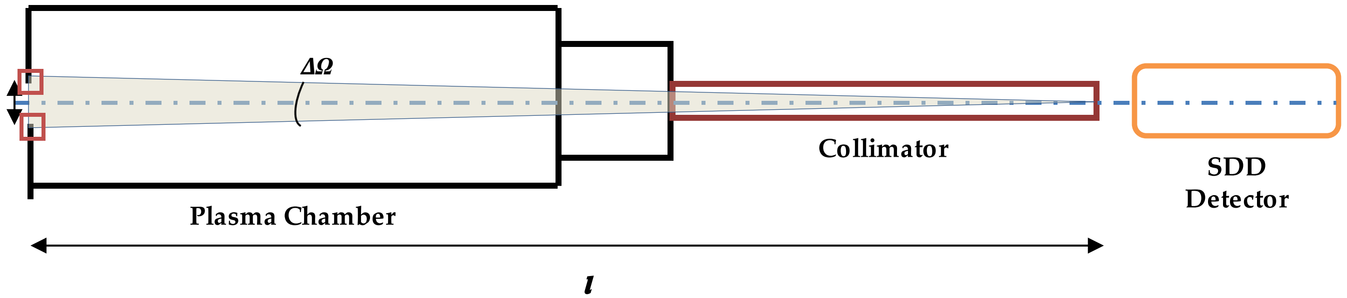

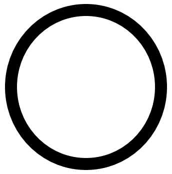

Active emission area = $4\pi\varepsilon_{gl}^2 - \pi d^2/4$

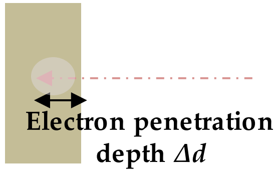

$$J_{theo,h\nu} = \frac{h\nu}{V_P \Delta E}\rho_{e,loss} N_t \int_I^{\infty} \sigma_{K,ion}(E) v_e(E) f(E) \mathrm{d}E$$

Deutsch-Mark formalism for K-shell ionisation cross-section

$$\sigma_{1s,ion} = g_{1s}\pi(r_{1s})^2 \xi_{1s} f(U) F(U)$$

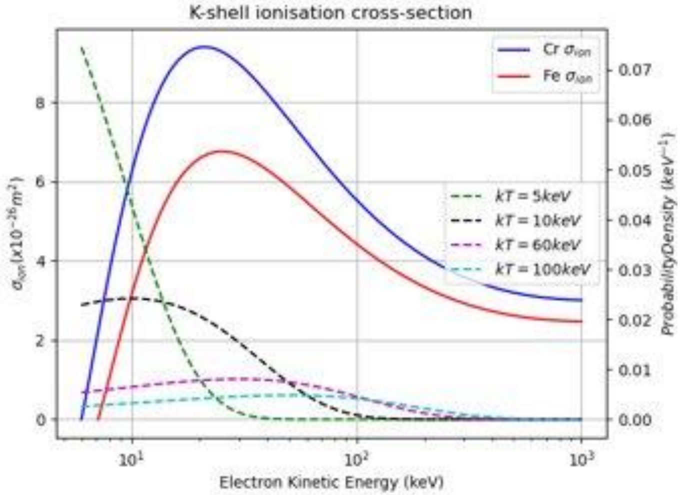

DM cross-section for Cr/Fe superposed on Maxwell EEDFs at different temperatures [6]

Estimation of number of target atoms N_t

$$N_t(E) = n_t\left(4\pi\varepsilon_g l^2 - \pi\frac{d^2}{4}\right)\Delta d(E)$$

Parametrisation of penetration depth as a function of energy

$$J_{theo,h\nu} = \frac{h\nu}{V_P \Delta E}\rho_{e,loss} n_t \left(4\pi\varepsilon_g l^2 - \pi\frac{d^2}{4}\right)\int_I^{\infty} v_e(E) f(E) \int_E^I \frac{1}{S(E)}\sigma_{K,ion}(E')\mathrm{d}E'\mathrm{d}E$$

$$J_{theo,line,loss}(h\nu) = \sum J_{theo,h\nu_0} D_{PV}(h\nu - h\nu_0, f_{h\nu_0})\Delta E$$

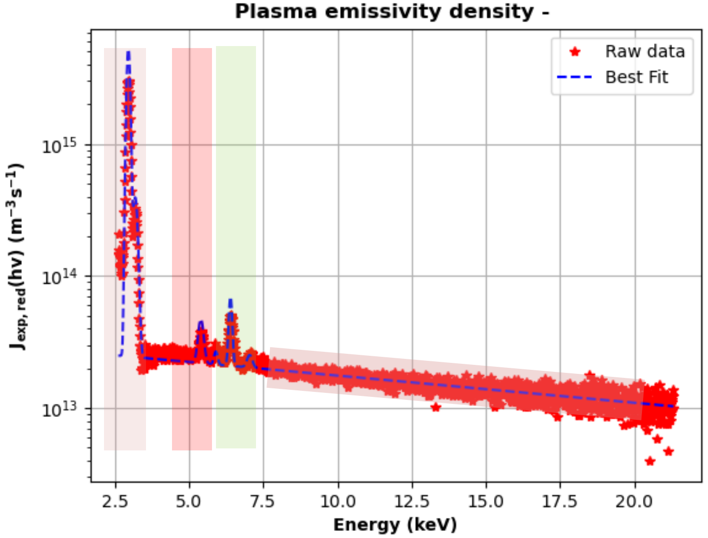

$\rho_e\rho_i$ ~ 1.32x10^{32} m^{-6}, expected ρe ~ 10^{16} m^{-3}

T_e ~ 21.15 keV

$\rho_{e,loss}$ ~ 10^{12} m^{-3}, estimated j_{av} ~ 2-3 mA/cm^2

Matches ion current density to order of magnitude

[6] B. Mishra *et al*, Phys. Plasmas, (2021)

Plasmas for Astrophysics Nuclear Decay Observation and Radiation for Archaeometry

Objective: Launch electron simulations for higher energy ranges and compare model-generated maps with experiment again

SECOND ATTEMPT
DATA: Debrecen 2018

Electron data stored in 7 new intervals:
[1,15], [15,29], [29,43], [43-57], [57,71], [71,85] and [85,∞] keV

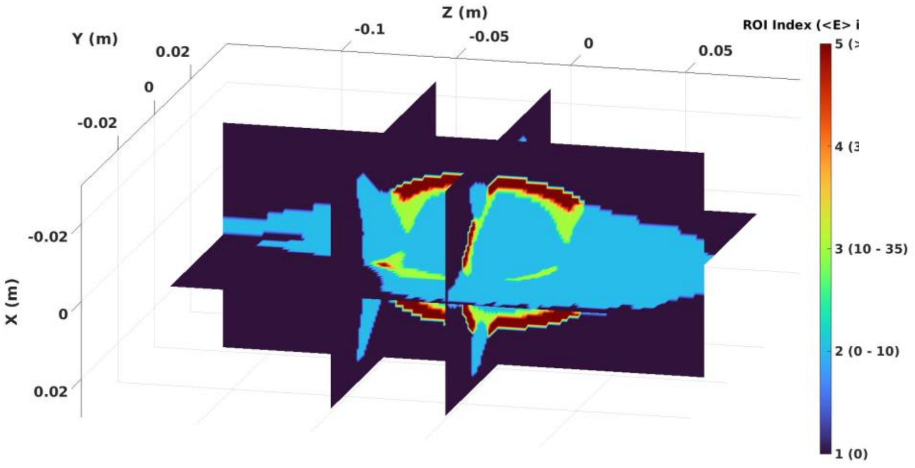

Mean electron energy-based ROIs generated for Debrecen 2018 plasma

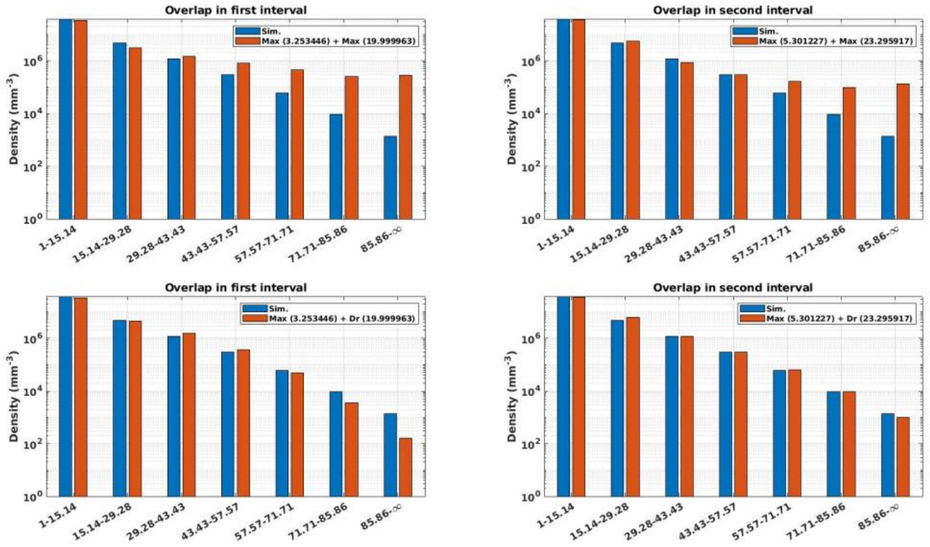

Qualitative EEDF fit of ROI 2 – best function Maxwellian+Druyvesteyn

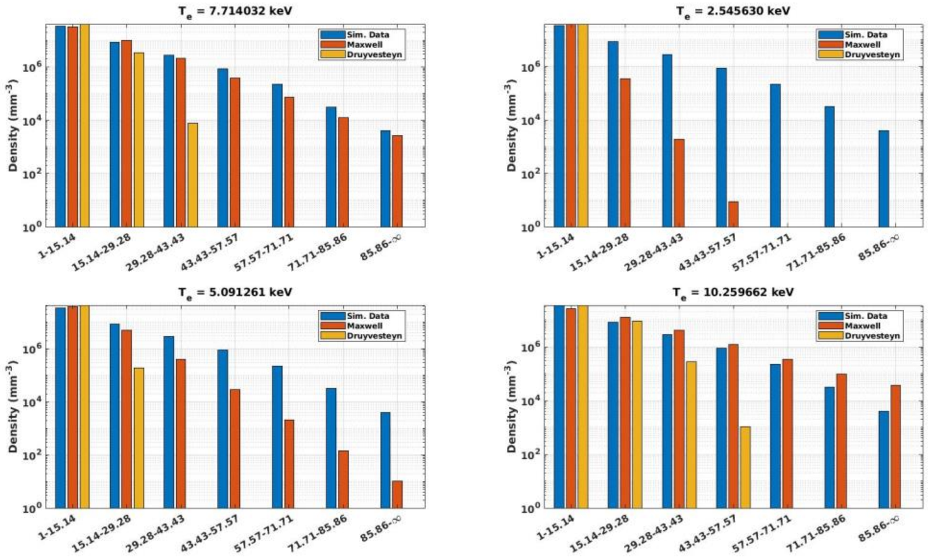

Qualitative EEDF fit of ROI 3 – best function Maxwellian

Electron Diagnostics – X-Ray Spectroscopy - Fluorescence

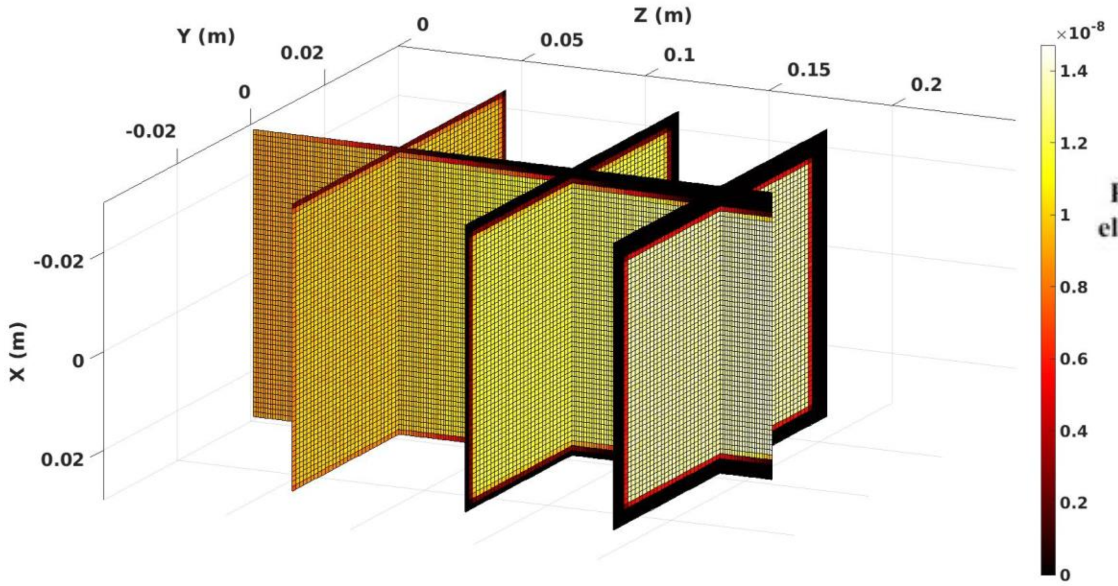

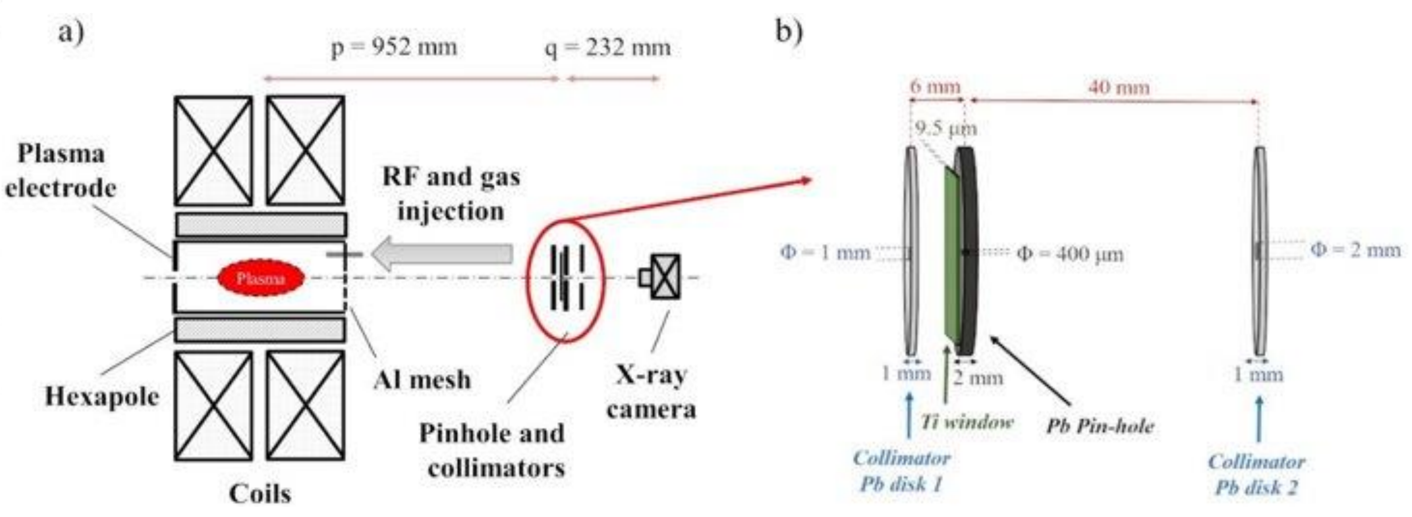

Schematic of multi-collimator CCD-pinhole setup used in Debrecen 2018 [9]

Local geometrical efficiency calculated using the ray-tracing Monte Carlo method without multi-collimator (top) and with multi-collimator (bottom) - enhanced screening and resolution

- 3D space-resolved charge density and EEDF
- K-shell ionisation cross-section
- Local geometrical efficiency

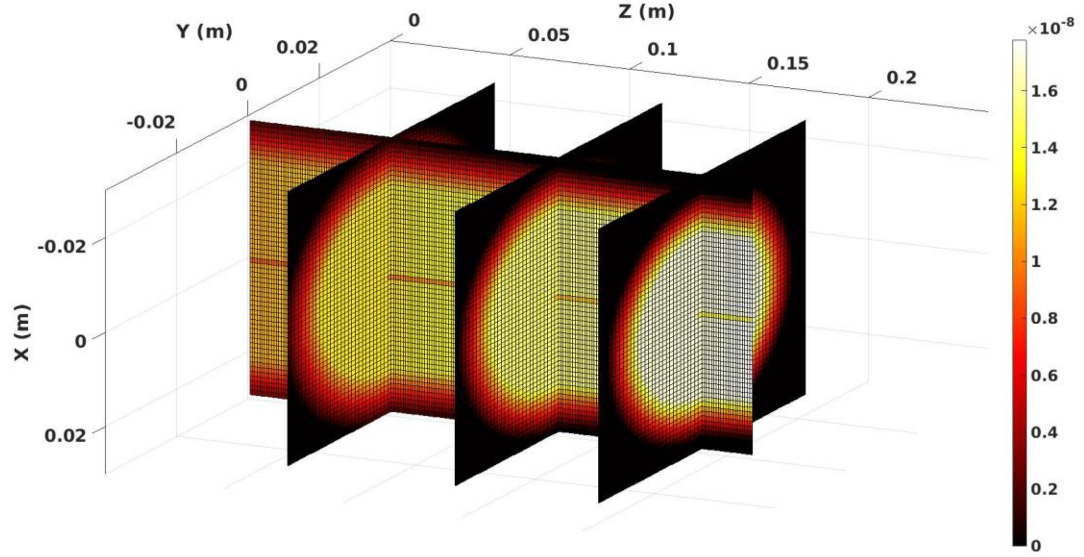

[9] S. Biri *et al*, JINST 16, P03003 (2021)

Electron Diagnostics – X-Ray Spectroscopy - Fluorescence

Space-resolved energy density + **K-Shell ionisation cross-section** + **Local geometrical efficiency**

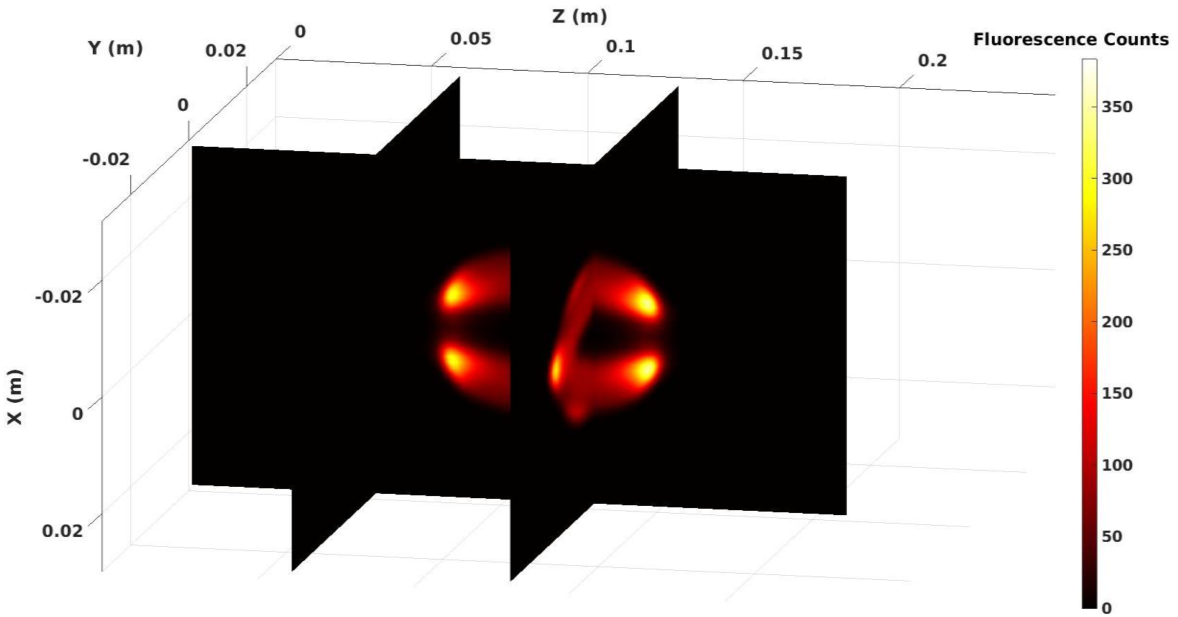

Simulated emission map from Debrecen 2018 configuration

Generating image of X-ray map on CCD – 1024x1024 pixels

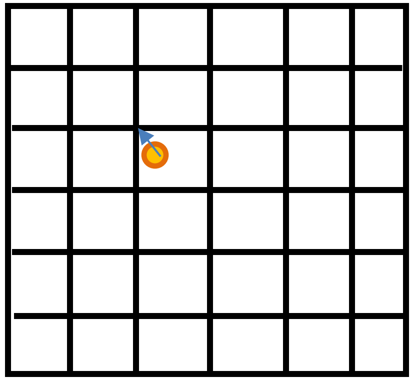

Grid of 1024 x 1024 points
Map photon to nearest grid point (0th order approximation)

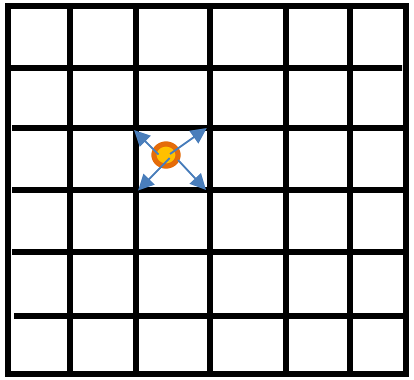

Grid of 1024 x 1024 points
Map photon to nearest neighbour grid points (1st order approximation)

Electron Diagnostics – X-Ray Spectroscopy - Fluorescence

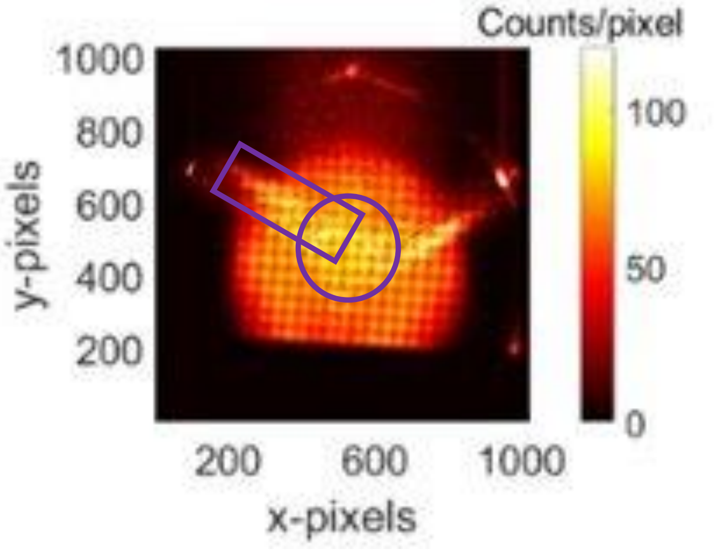

Experimental fluorescence map [9]

1st order projection

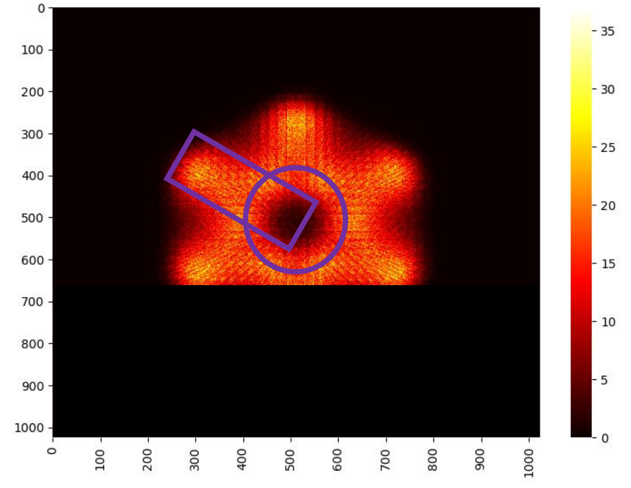

0th order projection

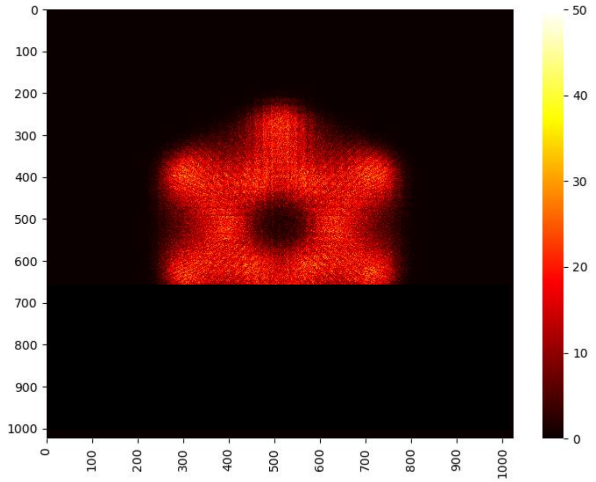

Conclusions:

New method for resolving plasma non-homogeneity established, allowing quantitative study of EEDF on a ROI-by-ROI basis

Match between experiment and model much better for Debrecen 2018 as compared to Debrecen 2014 – electron density on correct order of magnitude, general features reproduced

Some aspects not reproduced – notably the hole in the centre – can be attributed to incompleteness of electron simulations

Only 3 magnetic branches visible in experiment – may be attributed to ion density distribution, incomplete implementation of clusterisation

Upgrades underway:

- Update PIC code to generate realistic electron and ion maps
- New correct emission rates using space-resolved EEDFs
- Implement features like mesh and clustering in CCD projection
- Formalism to obtain fluorescence + bremsstrahlung from specific regions at CCD for more complete benchmarking

[9] S. Biri *et al*, JINST 16, P03003 (2021)

Ion Modelling – PIC-MCC

Objective: Develop Particle-in-Cell code to model 3D CSD and LPD profile of ions

BUFFER IONS BALANCE EQUATION:

$$\frac{dn_i}{dt} = \boxed{n_{i-1} n_e \gamma_{i-1,i}} - \boxed{n_i n_e \gamma_{i,i+1}} + \boxed{n_{i+1} n_0 E_{i+1,i}} - \boxed{n_i n_0 E_{i,i-1}} - \frac{n_i}{\tau_i}$$

KEYWORD(S): Steady state

The contribution from each process can be evaluated independently to construct CSD

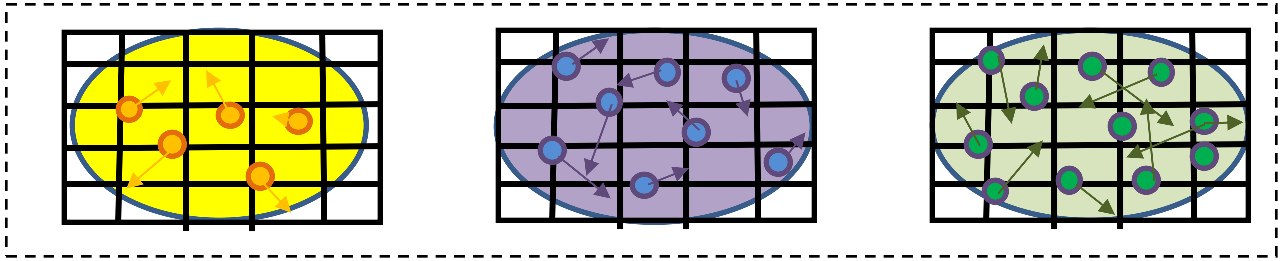

L_1 L_2 L_3

Particle transport under EM fields with collision to generate 3D spatial distribution (occupation maps)

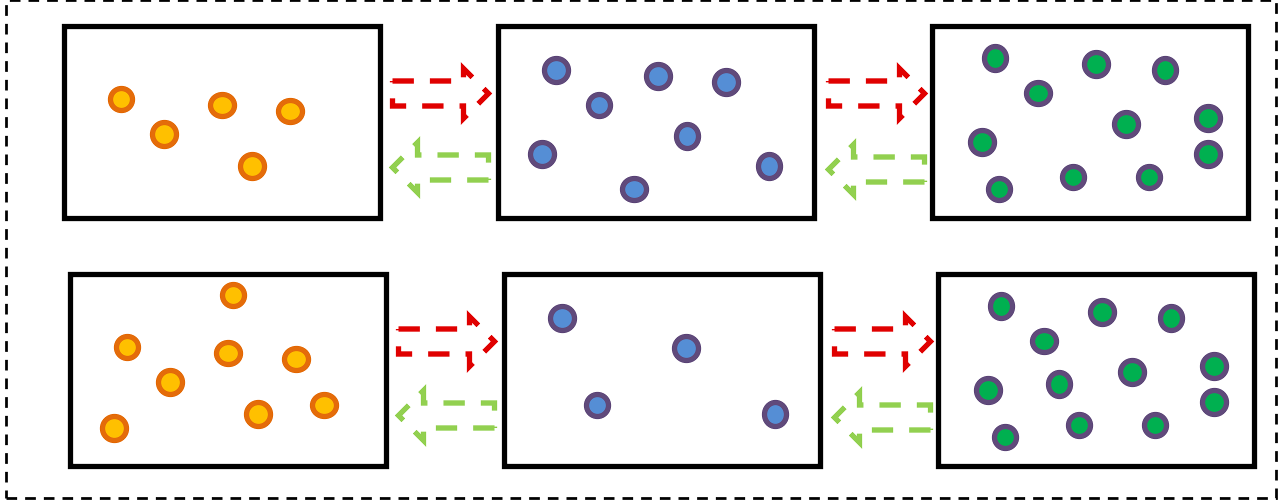

$t = t_1$

$t = t_2$

$W_1 = N_{L1}/N_{tot}$ $W_2 = N_{L2}/N_{tot}$ $W_3 = N_{L3}/N_{tot}$

Constant monitoring of loss/gain of macroparticles between various levels to calculate relative weight of each level

Forward reactions – ionisation, excitation, absorption
Backward reactions – charge exchange, de-excitation, spontaneous emission

N macroparticles
Initial r, v, reaction parameters
B field
ION, CEX and OCC maps

↓

Set T_{span} and T_{step}

↓

Begin iteration t=0

Ionisation → Update ION
Exchange → Update CEX
Neither → Update OCC

↓

$t=\tau_{p\_2}$

$n_i \rightarrow \rho_i \rightarrow \Delta\rho \rightarrow$ Calculate E_{DL}

Ionisation → Update ION
Exchange → Update CEX
Neither → Update OCC

↓

$t=\tau_{p\_2}$

⋮

End iteration t=T_{span}

Save Occ, Ion, CEX maps and transfer coefficients

[10] B. Mishra *et al*, Frontiers in Physics 10:932448

Buffer Ion PIC Code – Preliminary Benchmarks

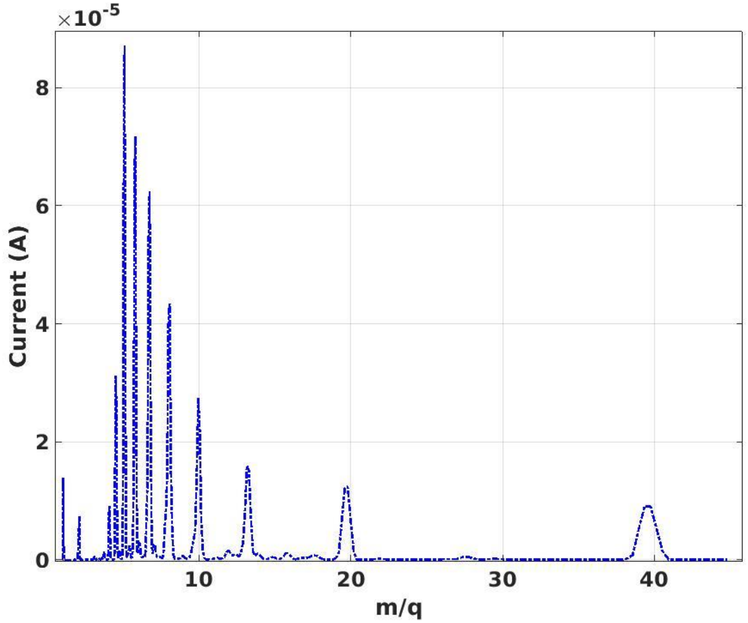

Experimental spectrum of Ar ion current [14]

$$I_i = \kappa \frac{(2L)S}{2}\,\frac{\langle N_i\rangle q_i e}{\tau_i}$$

$$\tau_{ES,i} = R\frac{\sqrt{\pi}L}{\nu_i}\exp\left(\frac{q_i e\langle\phi_{DL}\rangle}{k_B T_i}\right)$$

$$\tau_{d,i} = 7.1\times 10^{-20} L q_i \ln\Lambda\sqrt{A}\,\frac{n_e Z_{eff}}{k_B T_i^{3/2} E}$$

$$\frac{1}{\tau_i} = \frac{1}{\tau_{ES,i}} + \frac{1}{\tau_{d,i}}$$

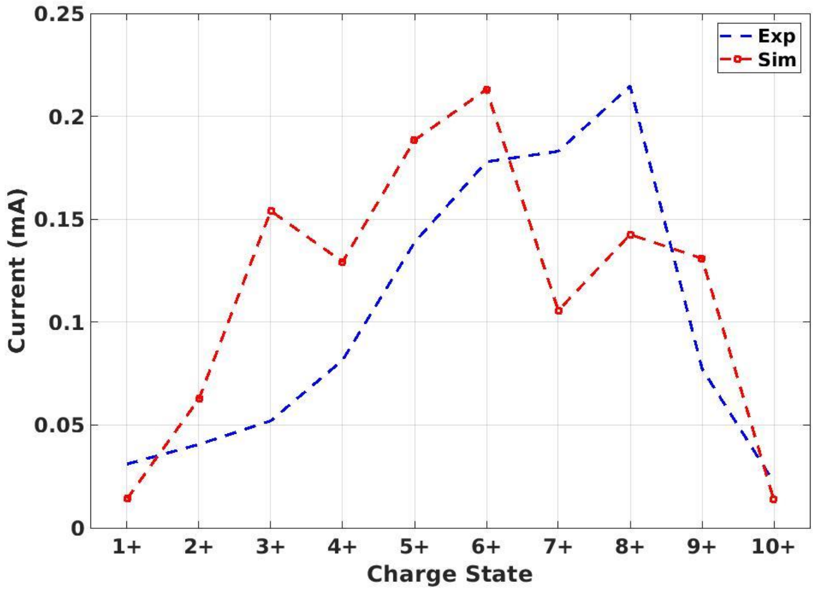

Simulated spectrum of Ar ion current with ambipolar diffusion and double layer confinement

L = 105 mm

Φ_{ext} = 11 mm

<N_i> = Mean density in region of potential dip

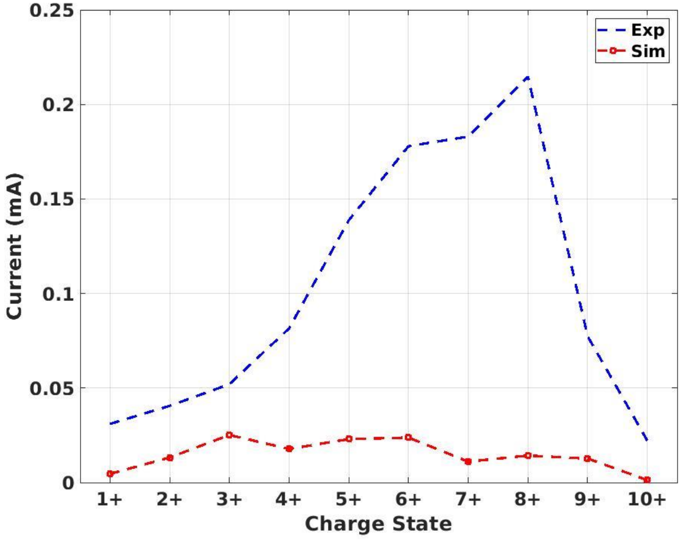

Simulated spectrum of Ar ion current with ambipolar diffusion alone

Upgrades underway:

- **Benchmarking with exact experimental parameters and precise evaluation of <N_i>**

[10] B. Mishra *et al*, Frontiers in Physics 10:932448

[14] S. Biri *et al*, Rev. Sci. Instrum. 83, 02A431 (2012)

Buffer Ion PIC Code – Preliminary Electrostatic Field

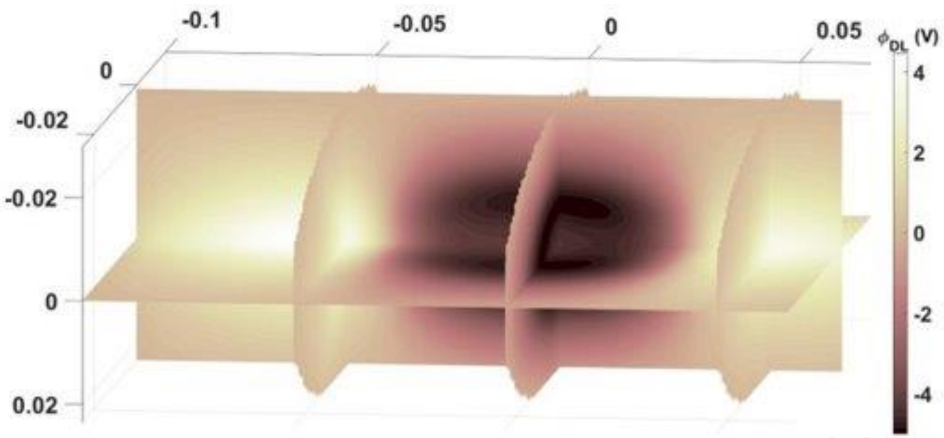

3D distribution of electrostatic potential showing potential dip [10]

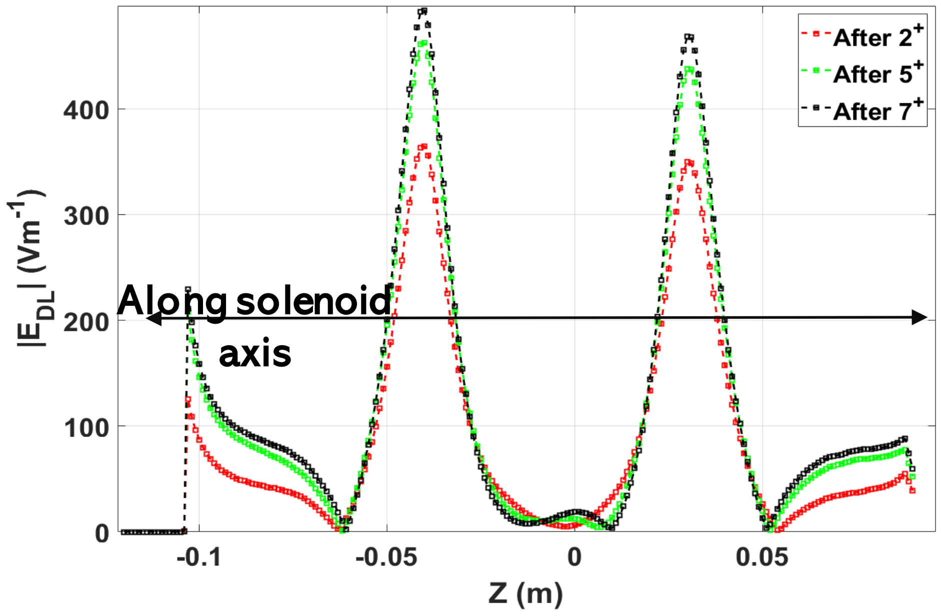

1D profile of double layer field along solenoid axis [10]

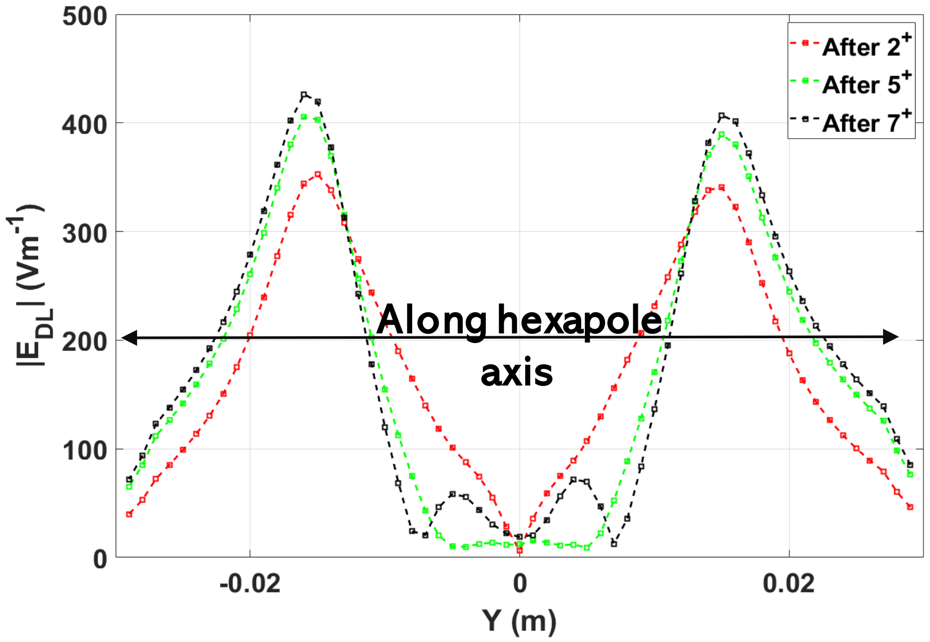

1D profile of double layer field along hexapole axis [10]

Upgrades underway:

- **Self-consistent evaluation of electrostatic field and potential dip**

[10] B. Mishra *et al*, Frontiers in Physics 10:932448